EDDY VISCOSITY-INTERMITTENCY FACTOR APPROACH TO NUMERICAL CALCULATION OF TRANSITIONAL HEATING ON SHARP CONES IN HYPERSONIC FLOW

John C. Adams, Jr.

ARO, Inc.

November 1970

VON KÁRMÁN GAS DYNAMICS FACILITY
ARNOLD ENGINEERING DEVELOPMENT CENTER
AIR FORCE SYSTEMS COMMAND
ARNOLD AIR FORCE STATION, TENNESSEE

NOTICES

EDDY VISCOSITY-INTERMITTENCY FACTOR APPROACH TO NUMERICAL CALCULATION OF TRANSITIONAL HEATING ON SHARP CONES IN HYPERSONIC FLOW

John C. Adams, Jr.

ARO, Inc.

FOREWORD

The work reported herein was sponsored by Headquarters, Arnold Engineering Development Center (AEDC), Air Force Systems Command (AFSC), under Program Element 62201F, Project 8953, Task 03.

The results of research presented were obtained by ARO, Inc. (a subsidiary of Sverdrup & Parcel and Associates, Inc.), contract operator of AEDC, AFSC, Arnold Air Force Station, Tennessee, under Contract F40600-71-C-0002. The research was conducted from July 1969 until March 1970 under ARO Project No. VW5006, and the manuscript was submitted for publication on June 26, 1970.

The author wishes to acknowledge the capable assistance of G. E. Gilley, ARO, Inc., who wrote the digital computer program used in the present research. The author also wishes to thank M. Brown, Jr., ARO, Inc., for his help in performing the numerical calculations.

This technical report has been reviewed and is approved.

David C. Reynolds
Captain, USAF
Research and Development
   Division
Directorate of Technology

Harry L. Maynard
Colonel, USAF
Director of Technology

ABSTRACT

Analysis of laminar, transitional, and turbulent boundary layers on a sharp cone at zero angle of attack under hypersonic perfect gas conditions is presented. The governing boundary-layer equations were numerically integrated on a digital computer using a marching, iterative, implicit, finite-difference method. The turbulent boundary layer is analyzed using a two-layer eddy viscosity model with a constant turbulent Prandtl number, and the transition region is treated through an eddy viscosity-intermittency factor approach. Comparison with experimental data reveals that the present approach yields an accurate description of laminar, transitional, and fully turbulent heat transfer on sharp cones in the Mach number range from 5 to 10 under cold wall conditions. Verification of the detailed calculation of transitional and turbulent boundary-layer structure under hypersonic conditions must await further experimental investigations. It appears at the present time that the eddy viscosity approach to calculation of transitional and turbulent boundary layers may indeed be applicable and accurate under hypersonic conditions.

CONTENTS

APPENDIXES

I. ILLUSTRATIONS

NOMENCLATURE

$A*$	van Driest damping constant, 26.0
A_n, B_n, C_n	Coefficients in finite-difference Eq. (III-24)
Cf_∞	Skin friction coefficient, $2\tau_w/\rho_\infty U_\infty^2$
C_p	Constant pressure specific heat, 6006 ft^2/sec^2 - °R
D_1, D_2	Coefficients for finite-difference derivatives defined by Eqs. (III-20) and (III-21)
E_n	Coefficient in finite-difference Eq. (III-29)
e_n	Coefficient in finite-difference Eq. (III-29)
f	Transformed stream function
f'	Velocity ratio, $\bar{u}/U_e$
f''	Velocity gradient, $\partial(\bar{u}/U_e)/\partial\eta$
g	Stagnation temperature ratio, $\bar{T}_0/\bar{T}_{0,\infty}$
h'	Fluctuation in static enthalpy
$\bar{h}$	Mean static enthalpy
I_f	Intermittency factor
j	Flow index, 0 (two-dimensional flow) and 1 (axisymmetric flow)
K	Variable grid parameter defined by Eq. (III-22)
k	Thermal conductivity
$k*$	Inner law mixing length constant, 0.435
L	Slant height of sharp cone
ℓ^*	Modified density-viscosity product ratio for use in momentum equation
ℓ^{**}	Modified density-viscosity product ratio for use in energy equation
ℓ_*	Mixing length
ℓ	Density-viscosity product ratio, $\rho\mu/\rho_e\mu_e$
M	Mach number
M_e	Local edge Mach number

M_∞	Free-stream Mach number
N	Total number of grid points
n	Exponent for power-law profiles
Pr	Laminar Prandtl number, 0.71
Pr_t	Turbulent Prandtl number, 0.90
p	Static pressure
p_0'	Free-stream pitot pressure
$p_{0,\infty}$	Reservoir stagnation pressure
p_t	Pitot pressure in boundary layer
$\dot{q}$	Heat flux
R	Specific gas constant, 1716 ft^2/sec^2 - °R
R_n	Coefficient in finite-difference Eq. (III-24)
$Re_{e,x}$	Local Reynolds number, $\rho_e U_e x / \mu_e$
$Re_{\infty,x}$	Free-stream Reynolds number, $\rho_\infty U_\infty x / \mu_\infty$
r_b	Body radius
r_f	Recovery factor
$St_{e,aw}$	Local Stanton number based on adiabatic wall conditions, $\dot{q}/\rho_e U_e C_p (T_{aw} - T_w)$
$\bar{T}$	Mean static temperature
T_{aw}	Adiabatic wall temperature
T_e	Static temperature at outer edge of boundary layer
$\bar{T}_0$	Mean stagnation temperature
$T_{0,\infty}$	Reservoir stagnation temperature
T_w	Wall temperature
U_e	Tangential velocity component at outer edge of boundary layer
U_∞	Free-stream velocity
u'	Fluctuation in tangential velocity component
$\bar{u}$	Mean tangential velocity component
V	Combined normal velocity components according to Eq. (7)

v'	Fluctuation in normal velocity component
$\overline{v}$	Mean normal velocity component
W	Dependent variable in finite-difference Eq. (III-8)
X_T	Surface distance from apex to beginning of fully turbulent flow
X_t	Surface distance from apex to onset of transition location
x	Coordinate along body surface
y	Coordinate normal to body surface
y_ℓ	Characteristic thickness of boundary layer in Eq. (21)
$\alpha_1, \alpha_2, \alpha_3, \alpha_4$	Standard form coefficients for parabolic, partial, differential equation following Eq. (III-3)
β	Velocity gradient parameter defined by Eq. (49)
γ	Specific heat ratio, 1.40
δ	Boundary-layer thickness (y distance where $f' = 0.995$)
δ_v	Cone half-angle
ϵ	Eddy viscosity
θ	Static temperature ratio, $\overline{T}/T_e$
θ'	Static temperature gradient, $\partial(\overline{T}/T_e)/\partial\eta$
κ	Eddy thermal conductivity
λ	Outer law mixing length constant, 0.090
μ	Laminar (molecular) viscosity
ξ, η	Transformed coordinates defined by Eqs. (36) and (37)
ρ'	Fluctuation in mass density
$\overline{\rho}$	Mean mass density
ρ_e	Mass density at outer edge of boundary layer
ρ_∞	Free-stream mass density
τ	Shear stress
τ_w	Wall shear stress
ϕ	Intermittency factor constant, 0.412
χ	Characteristic extent of transition zone defined by Eq. (29)

ψ	Stream function
Ω	Initial η step-size increment defined by Eq. (III-23)

SUBSCRIPTS

aw	Adiabatic wall
e	Outer edge of boundary layer
o	Stagnation or total
o, ∞	Reservoir
ref	Reference value
w	Wall
∞	Free-stream condition

SUPERSCRIPTS

|	
´	Fluctuating quantity or partial derivative with respect to η depending on usage
—	Quantity averaged with respect to time

SECTION I
INTRODUCTION

The successful design and operation of a reusable lifting entry space-craft depends partly upon the design of the thermal protection system. In turn, the thermal protection system design depends primarily on the thermodynamic environment. Peak heat-transfer rates and duration of the heating are the most influential thermodynamic parameters. In general, the peak heat-transfer rate determines the thermal protection system materials, and the duration of heating and the integrated energy available determines the mass of the thermal protection system.

Boundary-layer transition to turbulence is well known to have a major influence on the magnitude of lifting entry body heating rates. Lifting entry trajectories, characterized by a gradual variation in altitude and velocity, magnify the influence of the transitional zone on local heating histories. The gradual variation of local conditions induces the location for transition onset to move forward at a slow rate. At a fixed location on the body, the fully turbulent heat-transfer rate decreases with time, causing peak turbulent heating to occur near the inception of fully turbulent flow. With different assumptions of the development time necessary to achieve fully turbulent flow, significant variances in local heating histories are possible. Hence, accurate predictions of peak heating rates and total integrated heating loads require a realistic model of the transition zone. The assumption of fully turbulent flow at a point where the flow is actually transitional can result in an overweight design of the thermal protection system, which cannot be tolerated because of the low ratio of payload to gross weight characteristic of lifting entry vehicles. This subject has been the topic of a recent paper by Masaki and Yakura (Ref. 1).

Prediction techniques for the nonsimilar fully turbulent hypersonic boundary layer utilizing large digital computer codes have become available during the past few years, e.g., Smith and Cebeci (Ref. 2), Patankar and Spalding (Ref. 3), Bushnell and Beckwith (Ref. 4), Herring and Mellor (Ref. 5), Martellucci, Rie, and Sontowski (Ref. 6), and Mayne and Dyer (Ref. 7). Comparison of results from the above analyses with experimental data have shown good agreement for fully turbulent hypersonic (up to $M_\infty \approx 10$) boundary layers on sharp and slightly blunted cones as well as sharp flat plates. These results suggest that the eddy viscosity model employing the Prandtl mixing length is indeed adequate for prediction of hypersonic turbulent boundary-layer flows over simple bodies under cold wall conditions and may be used with some confidence.

With regard to prediction of transitional boundary-layer flows, little has been accomplished. Most of the references above employ an instantaneous step transition from fully laminar to fully turbulent flow at either a specified body location or local Reynolds number along the boundary-layer edge. An illustration of this type of treatment is given in the sketch below.

Distance along Body
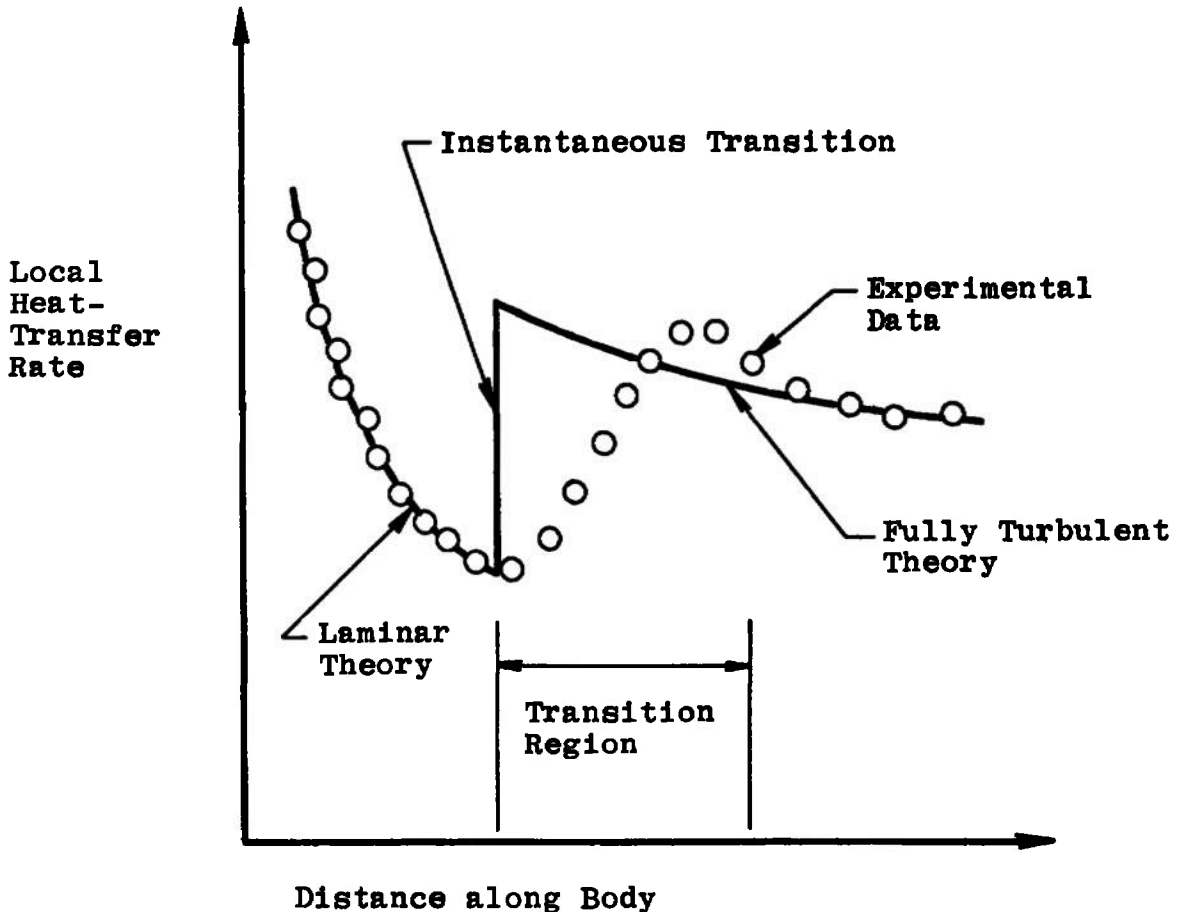
It is readily apparent that the instantaneous transition approach is not a valid model for the transition region. In order to provide a suitable progressive transition model, Masaki and Yakura (Ref. 1) propose an intermittency factor phenomenological description of the transition region based on the experimentally observed fact that transition in a boundary layer is characterized by the intermittent appearance of turbulent spots which grow and move downstream with the fluid. Although this approach appears to have merit, Masaki and Yakura present no results for the progressive transition model relative to experimental data. They state that the primary purpose of their paper is to encourage further studies on this subject.

The present work represents an adaptation of Masaki and Yukura's intermittency factor description of the transition region coupled with implicit finite-difference numerical solution of the governing turbulent boundary-layer equations for the case of hypersonic flow over a sharp cone at zero angle of attack. Since the current state-of-the-art in turbulent boundary-layer analysis under hypersonic conditions is very uncertain, comparison of theoretical predictions with experimental data is presented in order to establish the basic validity of the present approach. In general, the intermittency factor treatment used herein appears to yield a reasonably accurate description of transitional heating on sharp cones in hypersonic flow based on comparisons with experimental data. This finding says very little, however, about the detailed prediction of transitional and turbulent boundary-layer structure under hypersonic conditions which must await further experimental investigation.

The favorable results of the present study indicate that the intermittency factor approach coupled with numerical solution of the turbulent boundary-layer equations may be a powerful tool in analysis techniques for transitional heating on lifting body configurations. Much work remains to be done in this area.

SECTION II
THEORETICAL MODEL

The theory used herein is based upon numerical solution of the nonsimilar, compressible boundary-layer equations written in transformed variables using a marching, iterative, implicit finite-difference procedure. The turbulent transport terms in the boundary-layer equations are treated using a two-layer eddy viscosity model based on Prandtl's mixing length in conjunction with a modification of van Driest's analysis for the near-wall region. The transition zone is represented by an intermittency factor approach coupled to the eddy viscosity model.

2.1 GOVERNING BOUNDARY-LAYER EQUATIONS

The present analysis employs the compressible turbulent boundary-layer equations in terms of time-averaged mean flow quantities. With the following assumptions for the Reynolds stress and heat transfer

$$- \bar{\rho} \, \overline{u'v''} = \epsilon \, \frac{\partial \bar{u}}{\partial y} \tag{1}$$

$$- \bar{\rho} \, \overline{v'h'} = \kappa \, \frac{\partial \bar{T}}{\partial y} = \frac{\kappa}{C_p} \, \frac{\partial \bar{h}}{\partial y} \tag{2}$$

3

and the definition of the turbulent Prandtl number

$$Pr_t = \frac{C_p \epsilon}{\kappa} \tag{3}$$

the governing compressible boundary-layer equations describing the flow about two-dimensional and axisymmetric bodies at high Reynolds number and constant pressure across the boundary layer are (Refs. 2, 8, 9, and 10):

CONTINUITY

$$\frac{\partial}{\partial x}(\bar{\rho}\,\bar{u}\,r_b{}^j) + \frac{\partial}{\partial y}(\bar{\rho}\,V\,r_b{}^j) = 0 \tag{4}$$

STREAMWISE MOMENTUM

$$\bar{\rho}\,\bar{u}\,\frac{\partial \bar{u}}{\partial x} + \bar{\rho}\,V\,\frac{\partial \bar{u}}{\partial y} = -\frac{dp}{dx} + \frac{\partial}{\partial y}\left[\mu\left(1 + I_f\frac{\epsilon}{\mu}\right)\frac{\partial \bar{u}}{\partial y}\right] \tag{5}$$

ENERGY

$$\bar{\rho}\,u\,C_p\,\frac{\partial \bar{T}}{\partial x} + \bar{\rho}\,V\,C_p\,\frac{\partial \bar{T}}{\partial y} = \bar{u}\,\frac{dp}{dx} + \mu\left(1 + I_f\frac{\epsilon}{\mu}\right)\left(\frac{\partial \bar{u}}{\partial y}\right)^2$$

$$+ \frac{\partial}{\partial y}\left[k\left(1 + I_f\frac{\epsilon}{\mu}\frac{Pr}{Pr_t}\right)\frac{\partial \bar{T}}{\partial y}\right] \tag{6}$$

where

$$V = \bar{v} + \frac{\overline{\rho'\,v'}}{\bar{\rho}} \tag{7}$$

and the usual expressions for the mean and fluctuating parts of the variables are used, e. g.,

$$\rho = \bar{\rho} + \rho' \tag{8}$$

The exponent j is equal to zero in a planar case, and equal to unity for an axisymmetric case. The intermittency factor, I_f, and the eddy viscosity, ϵ, are discussed in greater detail later in this section. The

static pressure variation, p(x), is regarded as input to the problem and hence a known quantity as is customary in boundary-layer analyses. The coordinates are a curvilinear system in which x is distance along the surface measured from the stagnation point or leading edge. The dimension y is measured normal to the surface. Within the boundary layer, the velocity components in the x- and y-direction are u and v, respectively. The body radius (for an axisymmetric body) is r_b. See Fig. 1, Appendix I, for clarification of nomenclature relative to sharp cone geometry which is of sole interest in the present work.

If subscript w denotes wall and e denotes outer edge, the associated boundary conditions on the above-defined equations are:

MOMENTUM

$$\bar{u}(x,y=0) = 0 \qquad (9)$$

$$V(x,y=0) = 0 \qquad (10)$$

$$\lim_{y \to \infty} \bar{u}(x,y) = U_e(x) \qquad (11)$$

ENERGY

$$\bar{T}(x,y=0) = T_w(x) \qquad (12)$$

$$\lim_{y \to \infty} \bar{T}(x,y) = T_e(x) \qquad (13)$$

which reflect the requirements of no slip or mass injection (blowing or suction) at the wall as well as a prescribed wall temperature variation. The outer edge velocity, U_e, and static temperature, T_e, must be determined from, say, an inviscid analysis consistent with the imposed static pressure distribution.

In order to close the set of governing equations, it is further assumed that the gas is thermally and calorically perfect air having a constant specific heat ratio $\gamma = 1.40$ and obeying the equation of state

$$p = \bar{\rho}R\bar{T} \qquad (14)$$

where R = 1716 ft^2/sec^2- °R. Hence, under this assumption

$$\bar{h} = C_p \bar{T} \tag{15}$$

where C_p = 6006 ft^2/sec^2 - °R. The laminar viscosity, μ, is taken to obey Sutherland's law

$$\frac{\mu}{\mu_{ref}} = \frac{T_{ref} + 198.6}{\bar{T} + 198.6} \left(\frac{\bar{T}}{T_{ref}}\right)^{3/2} \tag{16}$$

where $\bar{T}$ must have units of °R and subscript ref denotes a reference condition. The laminar Prandtl number, Pr, is taken to be a constant value of 0.71 across the entire boundary layer.

2.2 TURBULENT TRANSPORT LAWS

The shear stress in a turbulent boundary layer is treated herein by the use of a two-layer, inner-outer model using Prandtl's mixing-length hypothesis and a modification of van Driest's analysis for the near-wall region. This results in a continuous distribution of the shear stress from the laminar value at the wall, through the fully turbulent region, reaching zero at the outer edge of the boundary layer. The energy transport in a turbulent boundary layer is treated in this work through the incorporation of the eddy conductivity, κ, into a turbulent Prandtl number, Pr$_t$, according to Eq. (3).

Following the usual treatment of the boundary-layer equations for a turbulent two-dimensional boundary layer, the effective shear stress may be written as

$$\tau = \mu \frac{\partial \bar{u}}{\partial y} - \bar{\rho} \, \overline{u'v'} \tag{17}$$

where the term $- \bar{\rho} \, \overline{u'v'}$ is called the Reynolds stress and represents the shear stress introduced by the turbulence. Using Prandtl's mixing length hypothesis for the Reynolds stress results in

$$- \bar{\rho} \, \overline{u'v'} = \bar{\rho} \, \ell_*^2 \left|\frac{\partial \bar{u}}{\partial y}\right|^2 \tag{18}$$

where ℓ_* is called the mixing length. Comparison of Eqs. (1) and (18) reveals

$$\epsilon = \bar{\rho} \, \ell_*^2 \left|\frac{\partial \bar{u}}{\partial y}\right| \tag{19}$$

which is the definition of the eddy viscosity, ϵ, for use in the governing boundary-layer equations.

After Escudier (Ref. 11), Patankar and Spalding (Ref. 3) recommend the following variation of the mixing length, ℓ_*, across the boundary layer

$$\ell_* = k_* y, \text{ for } 0 < y \leq \lambda y_\ell / k_* \tag{20}$$

$$\ell_* = \lambda y_\ell, \text{ for } \lambda y_\ell / k_* < y \tag{21}$$

where the values for the various numerical constants are taken to be $k_* = 0.435$ and $\lambda = 0.09$. The value of y at the point where the velocity in the boundary layer is equal to 0.99 of the velocity at the boundary-layer outer edge is used to define the distance y_ℓ. The above choices follow Patankar and Spalding and result in good agreement with the mixing-length model proposed by Maise and McDonald (Ref. 12) for compressible turbulent boundary layers.

By analogy with Stokes' solution for an infinite flat plate undergoing simple harmonic motion parallel to itself in an infinite fluid, van Driest (Ref. 13) concluded that in the vicinity of a wall the shear stress in a turbulent fluid should be of the form

$$\tau = \mu \frac{\partial \overline{u}}{\partial y} + \overline{\rho} \, k_*^2 y^2 \left[1 - \exp\left(\frac{-y \sqrt{\tau_w \, \overline{\rho}}}{\mu \, A_*} \right) \right]^2 \left(\frac{\partial \overline{u}}{\partial y} \right)^2 \tag{22}$$

which results in an exponential damping of the turbulent part of the shear stress as the wall is approached and yields exactly the laminar shear stress form, $\tau = \mu \dfrac{\partial \overline{u}}{\partial y}$, at the wall. Although Eq. (22) was originally developed for incompressible flow, it is applied in the present work to compressible flow by application of the suggestion by Patankar and Spalding (Ref. 3) that the local value of shear stress be used instead of the wall value as originally recommended by van Driest (Ref. 13). The constant A_* is taken to be 26.0 following van Driest (Ref. 13).

The turbulent Prandtl number as defined by Eq. (3), i.e.,

$$Pr_t = \frac{c_p \epsilon}{\kappa}$$

is physically a measure of the ratio of eddy viscosity to eddy conductivity, that is, the ratio of the turbulent transport of momentum to the

turbulent transport of heat. Since the flow in the outer region of a turbulent boundary layer shows some similarity to a turbulent wake flow, one may advance arguments that a realistic formulation of turbulent Prandtl number requires a separate expression for the inner and outer region just as in the eddy viscosity formulation. A recent review by Rotta (Ref. 14) indicates that the turbulent Prandtl number varies in magnitude from approximately 0.90 near the boundary-layer outer edge to approximately 2.0 near the wall. Much work remains to be done in defining the turbulent Prandtl number distribution as the review by Rotta points out. Hence, in the present work the turbulent Prandtl number is taken to remain constant at 0.90 across the entire boundary layer as recommended by Patankar and Spalding (Ref. 3). This choice of turbulent Prandtl number is consistent with the analyses of Patankar and Spalding (Ref. 3), Martellucci, Rie, and Sontowski (Ref. 6), and Mayne and Dyer (Ref. 7); Smith and Cebeci (Ref. 2) use a value of unity.

The constraint used to define the end of the inner region and the beginning of the outer region is the continuity of the eddy viscosity. From Eq. (22), the eddy viscosity in the inner region is

$$\epsilon_i = \bar{\rho} \, k_*^2 y^2 \left[1 - \exp\left(\frac{-y \sqrt{\tau \bar{\rho}}}{\mu A_*} \right) \right]^2 \left| \frac{\partial \bar{u}}{\partial y} \right| \tag{23}$$

whereas for the outer region

$$\epsilon_o = \bar{\rho} \, \lambda^2 \, y_\ell^2 \left| \frac{\partial \bar{u}}{\partial y} \right| \tag{24}$$

with the constants k_*, A_*, λ, and y_ℓ as defined previously. Note that the damping term in Eq. (23) reflects the application of the local shear stress as opposed to the wall shear stress of Eq. (22) as discussed previously. From the wall outward, the expression for the inner eddy viscosity applies until

$$\epsilon_i = \epsilon_o \tag{25}$$

at which time the outer eddy viscosity takes over. A schematic of this variation in terms of the mixing lengths is shown below.

$$\ell_* = \lambda y_\ell = 0.09\ y_\ell$$

$$\ell_* = k_* y = 0.435\ y$$

van Driest Damping
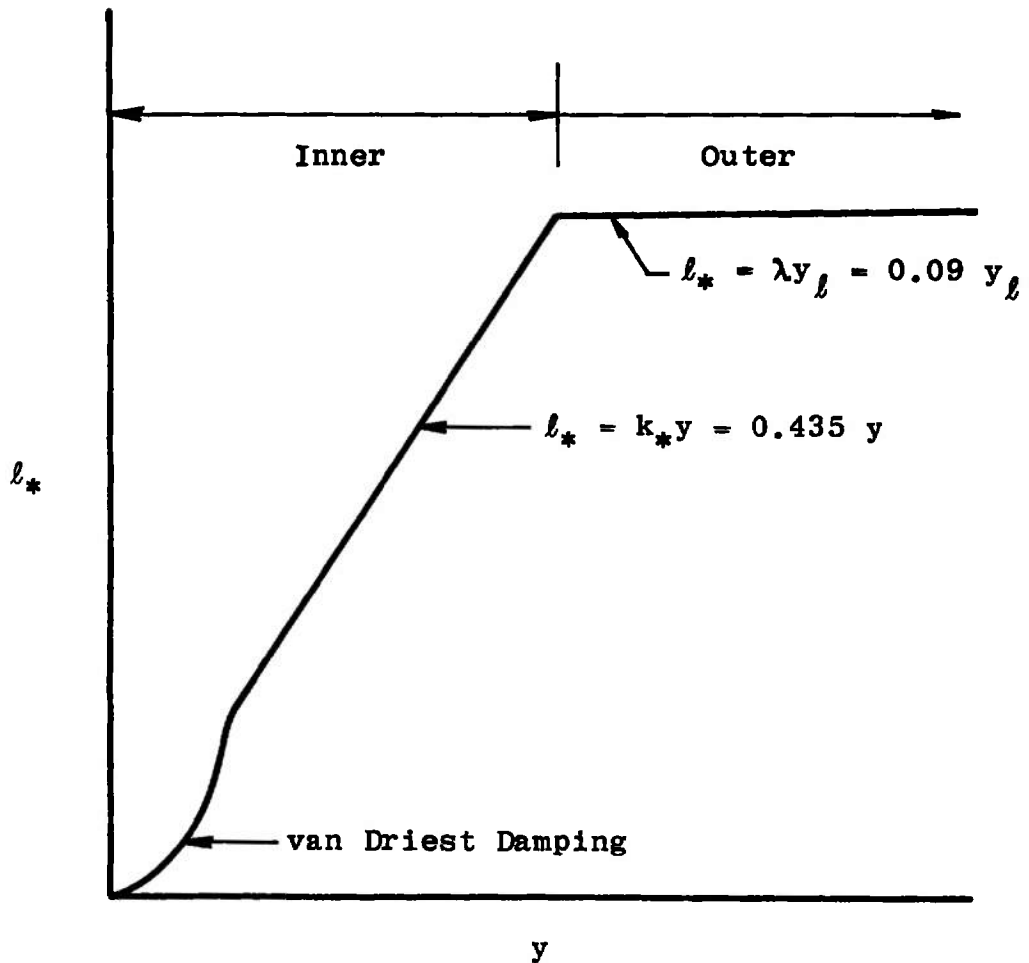
2.3 TRANSITION ZONE DESCRIPTION

The distance between transition onset at $x = X_t$ and the beginning of fully turbulent flow farther downstream at $x = X_T$ is denoted herein as the transition zone. In the present work, which is restricted solely to analysis of sharp cone flows, no attempt is made to predict, correlate, or otherwise _a priori_ infer the location of transition onset at X_t. Instead, the experimentally indicated beginning of the transition region is used for the onset point X_t based on the particular sharp cone heat-transfer data under examination.

Repeatability of gross characteristics of the transition region such as a nondimensional length have been observed in experimental investigations. Potter and Whitfield (Ref. 15) show that the transition zone local Reynolds number $Re_{e,\Delta x}$ (where $\Delta x = X_T - X_t$) has a dependence

on both transition onset local Reynolds number Re_{e,X_t} and the local Mach number M_e. In the present work, the extent of the transition zone will be represented by a transition zone local Reynolds number ratio $Re_{e,X_T}/Re_{e,X_t}$ which is related to $Re_{e,\Delta x}$ by

$$\frac{Re_{e,X_T}}{Re_{e,X_t}} = 1 + \frac{Re_{e,\Delta x}}{Re_{e,X_t}} \qquad (26)$$

where Re_{e,X_T} is the local Reynolds number at the inception of fully turbulent flow. The onset of transition, X_t, in the present work is determined from examination of experimental data as discussed previously. The end of transition is taken herein to coincide with the location of experimentally determined maximum heating. A schematic of this nomenclature is shown below.

Surface Distance along Body

10

+
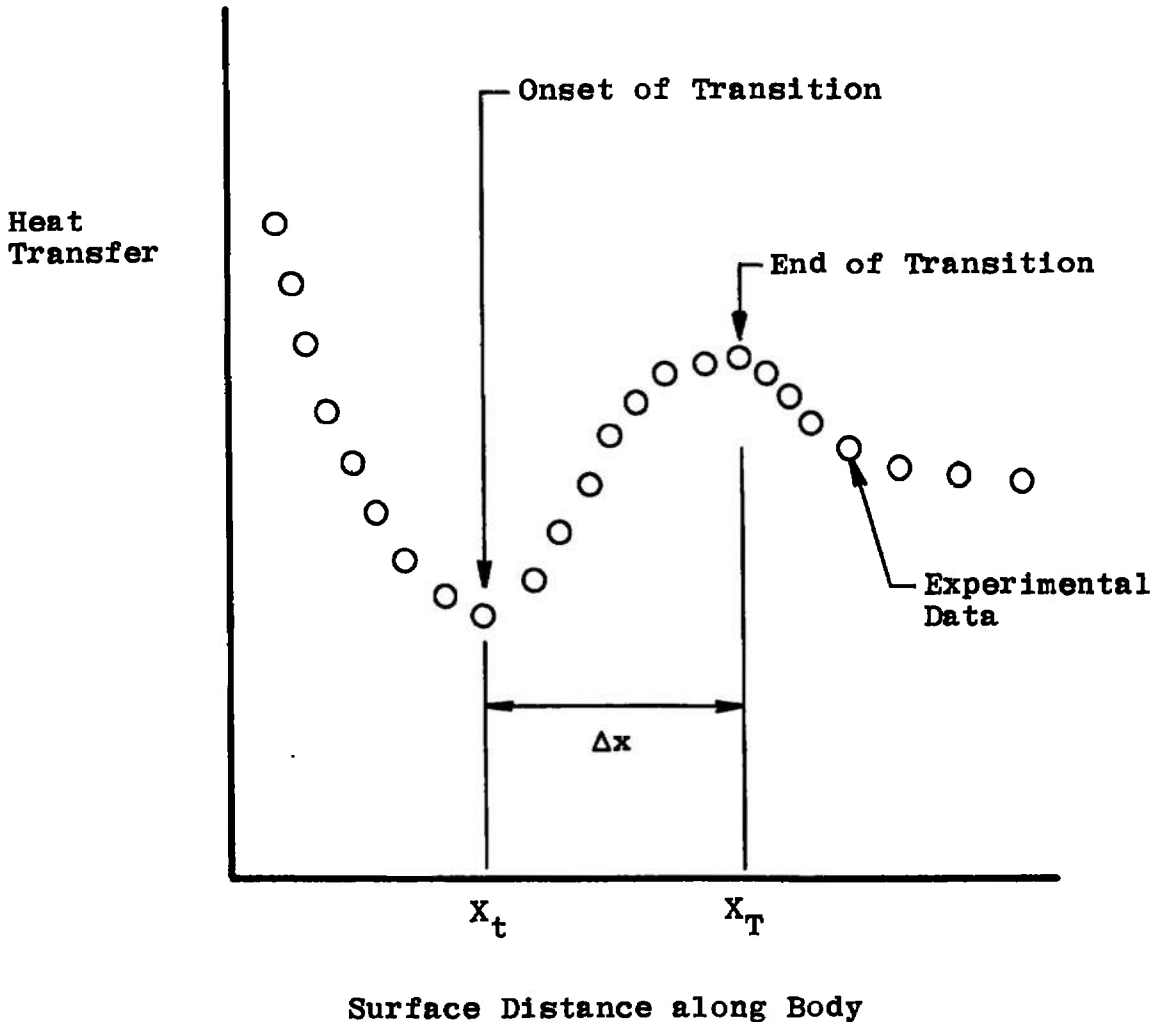
Masaki and Yakura (Ref. 1) present a comprehensive survey of un-classified experimental data showing transition on flat plates and cones over a range of local Mach number from 2 to 15. Based on this survey (which is given in Figs. 4 and 5 of their paper) they suggest that a value for $Re_{e,X_T}/Re_{e,X_t}$ of approximately 2 appears reasonable at high super-sonic speeds. The value of two is not a universal number, and a great deal of work remains to be done before this boundary-layer character-istic is fully understood. The effects of wall cooling and pressure gradi-ent are moot points at this time. It should be noted, however, that Murphy and Rubesin (Ref. 16) found that $Re_{e,X_T}/Re_{e,X_t} \approx 2$ based on flight test results from the Mark-2 blunt-nosed ballistic reentry vehicle. For the present work

$$\frac{Re_{e,X_T}}{Re_{e,X_t}} = 2 \tag{27}$$

following Masaki and Yakura (Ref. 1). As more hypersonic data become available, this factor of 2 may well require readjustment. For flows with pressure gradient and variable wall temperature the factor of 2 may not be applicable. All that can be said for its present use is that it appears reasonable based on available sharp cone and flat plate data from supersonic and hypersonic wind tunnel flows.

2.4 INTERMITTENCY FACTOR

In order to provide a suitable progressive transition model as opposed to an instantaneous transition model, the present analysis utilizes the phenomenological theory of the transition zone developed by Emmons (Ref. 17) which is based upon the experimental observation that transition in a boundary layer is characterized by the intermittent appearance of turbulent spots which grow and move downstream with the fluid. In the transition zone, the intermittent appearance of turbulent spots and their growth as they move downstream produces alterations of laminar and turbulent flow with a gradual increase in the mean turbulence level. At any point in the transition zone, the probability of turbulent flow is pre-scribed by a model based on the residence times of intermittent turbulent spots. Dhawan and Narasimha (Ref. 18) modified Emmons' original formu-lation of the probability of turbulent flow to account for a localized region of breakdown about $x = X_t$ in conjunction with a single universal intermit-tency distribution. The Dhawan and Narasimha model simply expresses the intermittency factor, I_f, which indicates the probability of the flow being turbulent at some point as

$$I_f(x) = 1 - \exp\left[-\phi\left(\frac{x - X_t}{x}\right)^2\right] \tag{28}$$

11

where ϕ is a constant equal to 0.412 and χ is a measure of the extent of the transition region characterized by

$$\chi = x]_{I_f = 0.75} - x]_{I_f = 0.25} \tag{29}$$

The beginning of the transition zone, where $I_f(0) = 0$, was established by Dhawan and Narasimha (Ref. 18) as being located at the transition onset distance $x = X_t$. In order to describe the extent of the transition zone, Masaki and Yakura (Ref. 1) assume that the end of transition is achieved at $x = X_T$ where

$$I_f(X_T) \geqq 0.97 \tag{30}$$

Substituting this assumption into Eq. (28) gives the length of the transition zone as

$$\Delta x = X_T - X_t = 2.96 \; \chi \tag{31}$$

In order to evaluate χ, recall that Eq. (27) mathematically defines the end of transition X_T in terms of the transition onset distance X_t as

$$Re_{e,X_T} = 2Re_{e,X_t} \tag{32}$$

which implies physically that the transition zone length Δx is equal to the transition onset distance X_t for the special case of supersonic or hypersonic flow over a sharp cone or sharp flat plate where the inviscid local flow parameters (p, T_e, ρ_e, U_e) remain constant over the entire body. Under this restriction

$$\Delta x = X_t \tag{33}$$

so that χ becomes, from Eq. (31)

$$\chi = \frac{X_t}{2.96} \tag{34}$$

With the above restrictions the intermittency factor given by Eq. (28) takes the final form

$$I_f(x) = 1 - \exp\left[-0.412 \; (2.96)^2 \left(\frac{x}{X_t} - 1\right)^2\right] \tag{35}$$

where

$$x \geqq X_t$$

Although the original derivation of the intermittency factor was based on experiments performed in low speed incompressible flow, Dhawan and Narasimha (Ref. 18) establish its validity for use in prediction of supersonic skin friction on a flat plate. To the author's knowledge, no work has been done on the effects of pressure gradients on the $I_f(x)$ distributions in either incompressible or compressible flows, although Dhawan and Narasimha speculate that pressure gradients would chiefly influence the manner of spot growth in the initial period near $I_f = 0$. Another point of interest is the distribution of I_f across the boundary layer, viz, normal to the surface. Dhawan and Narasimha state that although this $I_f(y)$ variation is probably of importance to the detailed structure of the turbulent motion, the value of I_f near the wall is the characteristic property of importance for the transition region and the $I_f(y)$ variation has only a secondary influence in determining the mean velocity profiles in transition. Hence, for the hypersonic sharp cone flows of interest in the present investigation, Eq. (35) is used for the intermittency factor distribution in order to assess its validity for use in such regimes.

In the present work the intermittency factor multiplies the eddy viscosity in the governing boundary-layer equations (5) and (6). This application follows Batchelor (Ref. 19) who found that this type of analytical treatment yielded the best agreement with experiments for the case of two-dimensional incompressible far wake flows where one is concerned with variations across the wake. The physical justification for using the intermittency factor in this manner lies in the basic physical definition of the intermittency factor as representing the fraction of time any point spends in turbulent flow, i.e., the probability of the flow being turbulent at a given point. If $I_f = 0$, the flow is completely laminar, but if $I_f = 1$, the flow is fully turbulent. The present treatment of the intermittency factor-eddy viscosity product in the governing equations simply means that the (fully turbulent) eddy viscosity is multiplied by a damping factor (the intermittency factor) in order to achieve a smooth and continuous variation from laminar to turbulent flow through the transition region. A similar approach has been used by Martellucci, Rie, and Sontowski (Ref. 6) who varied the eddy viscosity linearily with respect to distance through the transition zone. In a sense this may be considered an intermittency factor type of treatment where the intermittency factor is a linear function of distance. However, Martellucci, Rie, and Sontowski did not attempt to assess the validity of this approach; no results were presented of transition zone predictions relative to experimental data. In this respect the present work is the first, to the author's knowledge, concerning analytical techniques applicable to the transition region where the governing boundary-layer equations are numerically integrated on a digital computer yielding predictions which are then compared with experimental data in order to establish their validity.

13

2.5 COORDINATE TRANSFORMATION

In order to facilitate numerical integration of the governing boundary-layer equations (4), (5), and (6), it is convenient to transform them to a coordinate system that removes the singularity at x = 0 and stretches the coordinate normal to the flow direction, as is usually done in laminar flow. The coordinate transformation used in the present work is the well-known Lees-Dorodnitsyn (Ref. 9, p. 31) transformation. The new independent variables introduced are

$$\xi(x) = \int_0^x \rho_e \mu_e U_e r_b^{2j} \, dx \tag{36}$$

$$\eta(x,y) = \frac{\rho_e U_e r_b^j}{\sqrt{2\xi}} \int_0^y \frac{\bar{\rho}}{\rho_e} \, dy \tag{37}$$

and hence derivatives become

$$\frac{\partial}{\partial x} = \rho_e \mu_e U_e r_b^{2j} \frac{\partial}{\partial \xi} + \frac{\partial \eta}{\partial x} \frac{\partial}{\partial \eta} \tag{38}$$

$$\frac{\partial}{\partial y} = \frac{\bar{\rho} U_e r_b^j}{\sqrt{2\xi}} \frac{\partial}{\partial \eta} \tag{39}$$

Introducing a stream function $\psi(x, y)$ in such a manner as to identically satisfy the continuity equation (4)

$$\bar{\rho} \, \bar{u} \, r_b^j = \frac{\partial \psi}{\partial y} \tag{40}$$

$$\bar{\rho} \, V \, r_b^j = -\frac{\partial \psi}{\partial x} \tag{41}$$

and defining a transformed stream function $f(\xi, \eta)$ such that

$$\psi(x,y) = \sqrt{2\xi} \, f(\xi, \eta) \tag{42}$$

the governing boundary-layer equations (Eqs. (5) and (6)) become, in the transformed ξ, η plane:

MOMENTUM

$$(\ell^* \, f'') \div ff'' + \beta[\theta - (f')^2]$$

$$= 2\xi \left[f' \, \frac{\partial f'}{\partial \xi} - f'' \, \frac{\partial f}{\partial \xi} \right] \qquad (43)$$

ENERGY

$$\left(\frac{\ell^{**}}{Pr} \, \theta' \right)' + f\theta' + (\gamma-1)M_e^2 \, [\ell^* \, (f'')^2$$

$$- \beta\theta f'] = 2\xi \left[f' \, \frac{\partial \theta}{\partial \xi} - \frac{\partial f}{\partial \xi} \, \theta' + \frac{\theta f'}{T_e} \, \frac{dT_e}{d\xi} \right] \qquad (44)$$

with the new dependent variables

$$f' \, (\xi, \eta) = \frac{\bar{u}}{U_e} \qquad (45)$$

$$\theta(\xi, \eta) = \frac{\bar{T}}{T_e} \qquad (46)$$

where primes denote differentiation with respect to the independent variable η, i.e.,

$$f'' = \frac{\partial^2 f}{\partial \eta^2}$$

$$\theta' = \frac{\partial \theta}{\partial \eta}$$

The following definitions apply to the above equations

$$\ell^* = \frac{\overline{\rho\mu}}{\rho_e\mu_e} \left(1 + I_f \, \frac{\epsilon}{\mu} \right) \qquad (47)$$

$$\ell^{**} = \frac{\overline{\rho\mu}}{\rho_e\mu_e} \left(1 + I_f \, \frac{\epsilon}{\mu} \, \frac{Pr}{Pr_t} \right) \qquad (48)$$

15

$$\beta = \frac{2\xi}{U_e} \frac{dU_e}{d\xi} \tag{49}$$

$$M_e = \frac{U_e}{\sqrt{\gamma R T_e}} \tag{50}$$

where the inviscid momentum equation

$$\frac{dp}{dx} + \rho_e U_e \frac{dU_e}{dx} = 0 \tag{51}$$

has been used to relate the inviscid velocity U_e to the imposed inviscid static pressure.

The physical boundary conditions given by Eqs. (9) through (13) become, in the transformed variables:

MOMENTUM

$$f(\xi, \eta = 0) = 0 \tag{52}$$

$$f'(\xi, \eta = 0) = 0 \tag{53}$$

$$\lim_{\eta \to \infty} f'(\xi, \eta) = 1 \tag{54}$$

ENERGY

$$\theta(\xi, \eta = 0) = \theta_w(\xi) \tag{55}$$

$$\lim_{\eta \to \infty} \theta(\xi, \eta) = 1 \tag{56}$$

The local convective heat flux at the body surface ($y = 0$) is given by the well-known Fourier law

$$\dot{q} = - k_w \left. \frac{\partial \overline{T}}{\partial y} \right|_w \tag{57}$$

which becomes, in the transformed coordinates,

$$\dot{q} = \frac{- \ell_w \rho_e \mu_e U_e r_b^j C_p T_e}{Pr_w \sqrt{2\xi}} \theta'(\xi, \eta = 0) \tag{58}$$

where

$$\ell_w = \frac{\overline{\rho_w \mu_w}}{\rho_e \mu_e} \tag{59}$$

In a similar manner, the local wall shearing stress may be written in terms of the transformed coordinates as

$$\tau_w = \mu_w \left. \frac{\partial \overline{u}}{\partial y} \right)_w \tag{60}$$

$$= \frac{\ell_w \rho_e \mu_e U_e^2 \, r_b^j}{\sqrt{2\xi}} \, f''(\xi, \eta = 0)$$

Various nondimensional quantities of interest are defined as follows:

LOCAL REYNOLDS NUMBER BASED ON FREE—STREAM CONDITIONS

$$Re_{\infty, x} = \frac{\rho_\infty U_\infty x}{\mu_\infty} \tag{61}$$

LOCAL REYNOLDS NUMBER BASED ON INVISCID EDGE CONDITIONS

$$Re_{e, x} = \frac{\rho_e U_e \, x}{\mu_e} \tag{62}$$

LOCAL SKIN FRICTION COEFFICIENT REFERENCED TO FREE—STREAM CONDITIONS

$$C_{f_\infty} = \frac{\tau_w}{\frac{1}{2} \rho_\infty U_\infty^2} \tag{63}$$

LOCAL STANTON NUMBER BASED ON INVISCID EDGE CONDITIONS AND ADIABATIC WALL TEMPERATURE

$$St_{e, aw} = \frac{\dot{q}}{\rho_e U_e C_p \, (T_{aw} - T_w)} \tag{64}$$

17

where

$$\frac{T_{aw}}{T_{0,\infty}} = r_f + \frac{T_\infty}{T_{0,\infty}} (1 - r_f) \tag{65}$$

with r_f the recovery factor which must be defined relative to the flow under examination.

2.6 NUMERICAL SOLUTION

In the present work, numerical solution of the simultaneous, non-linear, parabolic, partial differential equations (Eqs. (43) and (44)) is performed by obtaining linear finite-difference equivalents of the equations and solving these using an iterative, marching, tridiagonal matrix method. Details of the finite-difference procedure are given in Appendix III.

The digital computer code is written in FORTRAN 63 for use on a CDC 1604-B machine. Solution time including printout is approximately 20 minutes on the 1604-B machine for a body divided into 100 stations. No numerical stability problems have been encountered with the present finite-difference approach because of its implicit nature.

Much debate currently exists about the relative merits of different numerical techniques for solution of the turbulent boundary-layer equations; a good example may be found in Paper 21 of Ref. 20 which is a written transcription of the verbal panel and general discussion portion of a 1968 symposium on compressible turbulent boundary layers. General reviews of this subject have been given by Spalding (Ref. 21), McDonald (Ref. 22), Beckwith (Ref. 23), and Smith (Ref. 24).

SECTION III
COMPARISON OF PRESENT NUMERICAL RESULTS WITH EXPERIMENTAL DATA

As pointed out by Smith (Ref. 24) in his recent review of boundary-layer research over the past decade, the ultimate test of any theoretical analysis of the turbulent boundary layer is the end accuracy (and not the intrinsic logic) since empiricism is involved. Hence, with this in mind, comparison of experimental data with the present eddy viscosity-intermittency factor approach to prediction of transitional heating under hypersonic conditions is mandatory. Since the current effort is limited

solely to sharp cone geometry, the following additional restrictions are imposed at this point in order to clearly define the experimental flow field for comparison with the analytical model:

1. Hypersonic flow at zero angle of attack.

2. Uniform free stream, i.e., no source flow effects.

3. Cold wall at constant uniform temperature.

4. Transition zone well defined by heat-transfer data.

Under the above restrictions, a review of unclassified, published literature on hypersonic sharp cone experimental investigations revealed the six acceptable sources (Refs. 25 through 30) listed in Table I, Appendix II. Although this list appears to be very meager, the majority of published investigations do not meet the rather stringent restrictions imposed above and hence must be eliminated on this basis. For example, the work by Nagamatsu and Sheer (Ref. 31) contains source flow effects, and the wall temperature is not uniform in the study by Everhart and Hamilton (Ref. 32); Stetson and Rushton (Ref. 33) present no usable heat-transfer data defining transition. By only using experimental data from Table I, meaningful comparisons between theory and experiment can be made with some confidence since the assumptions under which the analytical model is formulated match the restrictions placed on acceptable experimental data.

Table II lists the inviscid outer-edge conditions for input to the boundary-layer analysis corresponding to the various flows in Table I. The inviscid conditions are determined from numerical solution of the inviscid conical flow equations following Sims (Ref. 34) for a given sharp cone half-angle and free-stream Mach number. Consistent with the gas model adopted in Section 2.1, a perfect gas with $\gamma = 1.40$ is used in the inviscid analysis.

Of the data in Table I, the investigation by McCauley, Saydah, and Bueche (Ref. 25) is one of the best documented with respect to test conditions and analysis of data. The test was conducted in the Hypersonic Wind Tunnel (C) of the von Kármán Gas Dynamics Facility, Arnold Engineering Development Center, at a nominal Mach number of 10. Test conditions are given in Table I. The objective of the experimental investigation was to determine the effects of various diameter spherical trips on boundary-layer transition along sharp and spherically blunted cones. Figure 2 shows a comparison of results from the present theory relative to experimental heat-transfer measurements for both natural transition and roughness-induced transition. In general, the agreement between experimental data and results from the present theory is good.

The transition region is well defined by the present theory which, it should be recalled, requires that the location of onset to transition be prescribed as shown in Fig. 2. Both sets of experimental data presented in Fig. 2 clearly show a factor of about 2 in the ratio X_T/X_t as previously discussed in Section 2.4 and used in the present analytical model. For the tripped condition, note that fully turbulent flow exists over approximately half the cone but, for the natural transition condition, the flow remains transitional over the entire aft half of the body. It is the large extent of transitional flow in the latter case which poses the thermal design problem for lifting entry vehicles.

Since the agreement between results from the present theory and experiment as shown in Fig. 2 indicates that the present theory is indeed applicable to prediction of transitional heating on a sharp cone in hypersonic flow, it is now in order to examine certain details of the flow field. Figures 3 through 7 present calculated velocity, static temperature, Mach number, stagnation temperature, and pitot pressure profiles at three locations along the sharp cone for the roughness-induced transition condition where the onset of transition occurs at the body location $x/L = 0.24$. This choice of flow conditions has been made to permit presentation of laminar ($x/L = 0.20$), transitional ($x/L = 0.40$), and fully turbulent ($x/L = 0.80$) profiles; the station $x/L = 0.40$ for the transitional profile corresponds to approximately the location of calculated maximum heating in Fig. 2. The different character of the laminar and turbulent profiles is apparent. The transitional profiles exhibit a larger gradient in flow properties near the wall than do the fully turbulent profiles. This phenomenon is discussed in more detail later.

In order to present the differences between laminar profiles and fully turbulent profiles at a given body location, Figs. 8 and 9 show calculated velocity and static temperature distributions for the two types of flow at $x/L = 0.80$. Figure 8 reveals the much fuller turbulent profile relative to the laminar profile as expected, whereas Fig. 9 shows that the peak static temperature in the laminar boundary layer occurs much farther from the wall than the peak turbulent static temperature, about a factor of 3 in distance normal to the surface. This factor of 3 in location of peak static temperature is somewhat reflected in the thickness of the turbulent boundary layer being approximately twice the thickness of the laminar boundary layer as can be seen by close inspection of Figs. 8 and 9.

Another comparison of interest relative to laminar and transitional flow profiles near the onset of transition is presented in Figs. 10 and 11 for the station $x/L = 0.30$. The transition process to turbulent flow affects the entire profile. This observation is in quantitative agreement with the experimental observations of Maddalon and Henderson (Ref. 35) as well as Potter and Whitfield (Ref. 36) for natural transition.

In order to understand the profile behavior discussed above, one must keep in mind that the eddy viscosity-intermittency factor product governs the transitional and turbulent flow calculations in the current approach. Figure 12 gives the intermittency factor variation over the body as governed by Eq. (35), and Fig. 13 gives the calculated eddy viscosity-intermittency factor product distribution across the boundary layer at selected stations. As is apparent from Fig. 13, the eddy viscosity reaches its maximum value in the outer region of the boundary layer with $\epsilon \gg \mu$ for fully turbulent flow. Note that for sufficiently large values of x/L such that $I_f \approx 1$, the ratio ϵ/μ at a given y/L value in the wall region approaches a common value independent of the x location as may be seen by comparing the curves for x/L = 0.40 and 0.80 in Fig. 13 at values of y/L < 5.0 x 10^{-4}. In the transition region where $I_f < 1$, the value of the ϵ/μ ratio near the wall is approximately the fully turbulent value at the same y/L location scaled down by the I_f ratio. For example, at y/L = 5.0 x 10^{-4}, ϵ/μ = 0.14 for x/L = 0.30 and ϵ/μ = 0.68 for x/L = 0.80, a factor of approximately five difference. From Fig. 12, I_f = 0.20 at x/L = 0.30 and I_f = 1.0 at x/L = 0.80 which reveals the factor of five scaling noted above. Thus the effect of the intermittency factor in the wall region is simply a scaling of the ϵ/μ ratio. In the outer regions of the boundary layer where the change has been made from the inner to the outer expression for calculating the eddy viscosity, scaling of the ϵ/μ ratio is not applicable as can be seen by reference to Fig. 13. Hence the character of the transitional zone description in the present analysis as presented in Figs. 10 and 11 can be directly traced to the treatment of the eddy viscosity-intermittency factor product discussed above.

One well-documented phenomenon in transitional boundary-layer flows is the experimentally observed overshoot in peak heat-transfer rate near the end of transition relative to fully turbulent boundary-layer theory. Figure 14 shows a comparison of results from the present method of analysis using the eddy viscosity-intermittency factor treatment of transition and results using an instantaneous step transition from laminar to turbulent flow at a given location. The present method clearly shows an overshoot in heat-transfer rate. This overshoot in heat-transfer rate is attributable to the transitional profile behavior discussed previously in connection with Figs. 3 through 7. Similar comments apply to the wall skin friction coefficient as shown by Fig. 15. One important point to note from Fig. 14 is that the calculated heat-transfer rates relax to common downstream values irrespective of the transition zone treatment; the same is true for the wall skin friction coefficients as can be seen from Fig. 15. This behavior is to be expected because of the parabolic mathematical character of the governing boundary-layer equations. Further note, from Fig. 16, that the

instantaneous step transition treatment gives a larger value for the
boundary-layer thickness downstream than the present intermittency
factor-eddy viscosity approach. Sufficiently far downstream both
models give the same value.

One method often used by experimentalists to detect boundary-layer
transition is a pitot tube mounted close to the surface of the body. Fig-
ure 17 shows the calculated pitot pressure variation along the body at
two fixed locations normal to the surface. The variation through the
transition zone is well defined, and the general trends are similar to
those for the distributions of heat-transfer rate and skin friction coeffi-
cient from Figs. 14 and 15. Although the distance $y/L = 4.0 \times 10^{-4}$
may not be physically realistic from the standpoint of actually construct-
ing a working probe, the above results indicate that pitot pressure meas-
urements do indeed offer a valid means of detecting transition under
hypersonic cold wall conditions.

Another technique often used by the experimentalist is the measure-
ment of pitot pressure profiles across the boundary layer, which are
used in conjunction with the Crocco relation (Ref. 9, pp. 33 and 182)

$$\frac{\overline{u}}{U_e} = \frac{\overline{T}_0 - T_W}{T_{0,\infty} - T_W} \tag{66}$$

to infer velocity profiles. The Crocco relation (Eq. (66)) represents a
solution to the governing laminar and turbulent boundary-layer equations
for the special case of zero pressure gradient, constant wall temperature,
and both laminar and turbulent Prandtl numbers equal to unity. These
conditions are satisfied in the present analysis of hypersonic sharp cone
flows (except for the Prandtl number restriction). Figure 18 presents a
comparison of the present theory with the Crocco relation written in
terms of the present transformed variables as

$$g = g_W + f' (1 - g_W) \tag{67}$$

where

$$g = \frac{\overline{T}_0}{T_{0,\infty}} \tag{68}$$

$$g_W = \frac{T_W}{T_{0,\infty}} \tag{69}$$

with $f' = u/U_e$ from Eq. (45). In general the agreement is excellent
which indicates that the Prandtl number and the turbulent Prandtl num-
ber have only a small influence on the solution when expressed in this

form. It should be pointed out, however, that this observation is being made for cold wall conditions only.

The investigations by Wallace (Refs. 37 and 38) are an excellent example of the approach given in the previous paragraph. In order to assess whether calculated velocity profiles were laminar or turbulent, Wallace compared them with power law profiles of the form

$$\frac{\bar{u}}{U_e} = \left(\frac{y}{\delta}\right)^n \tag{70}$$

since turbulent boundary-layer profiles are usually associated with small values of n, typically n = 1/7 to 1/10. Figure 19 presents representative power-law profiles relative to the calculated velocity profile from the present theory at a body location x/L = 0.80 where a fully turbulent boundary layer is present. Above $y/\delta = 0.20$, the present theory is seen to agree closely with the n = 1/5 power law. It is interesting to note in this respect that Pinckney (Ref. 39) found that a 1/5 power law velocity profile yielded good agreement with experimental static temperature-velocity profiles for flat plate compressible turbulent boundary layers with heat transfer in the free-stream Mach number range from 0.85 to 8.18.

So far the present work has been devoted to an analysis of one particular sharp cone flow under hypersonic conditions. Returning to the experimental data in Table I, it is now in order to compare results from the present theory with the remaining data. In all cases the comparisons will be made in terms of the same parameters given in the references so as to avoid error in reduction of data to a different form.

Shown in Fig. 20 is a comparison of a heat-transfer rate parameter calculated using the present theory with the data presented by DiCristina (Ref. 26) for Mach 10.2 hypersonic flow. This test was conducted in the Hypersonic Wind Tunnel (C) of the von Kármán Gas Dynamics Facility, Arnold Engineering Development Center; test conditions are given in Table I with corresponding inviscid edge conditions in Table II. Agreement of results from the present theory and experiment is excellent. A transition zone length equal to X_t is clearly seen in these data obtained under conditions for which natural transition occurred.

Figure 21 presents the experimental data of Sanator, DeCarlo, and Torrillo (Ref. 27) and results from the present theory. This test was performed in the 36-in. hypersonic wind tunnel at the Republic Aviation Corporation; test conditions are given in Table I with corresponding inviscid edge conditions in Table II. Spherical roughness elements were

used to trip the boundary layer in this test, with the location of these elements shown in Fig. 21. Again, the agreement of results from the present theory and experiment is excellent with fully turbulent flow being established over approximately half the cone. The transitional zone appears well defined by the present theory.

A very extensive program for measurement of hypersonic turbulent heat transfer on a highly cooled sharp cone has been under way for several years at the United States Naval Ordnance Laboratory using their Mach 5 hypersonic wind tunnel. The results of these investigations have been published in reports by Wilson and Fisher (Ref. 28) and Wilson (R Figure 22 shows a comparison of results from the present theory with experimental data from Fig. 6a of Ref. 28 and Fig. 13c of Ref. 29; test conditions and inviscid outer edge conditions are given in Tables I and II, respectively. As shown in Table I, the test conditions are almost identical for the two sets of data. The results from the present theory agree best with the data from Ref. 29 in the fully turbulent region whereas the data from Ref. 28 appear to best define the beginning of the transition region. Since the two sets of data are not mutually consistent it is difficult to assess if indeed the present theory is overestimating the fully turbulent heat-transfer rate for these flow conditions. Comparisons not presented herein of results from the present theory with other experimental data in Refs. 28 and 29 for different flow conditions reveal that in all cases the present theory gives values higher than the experimental data. It should be noted that Mayne and Dyer (Ref. 7) also obtained higher values than the fully turbulent experimental data from Ref. 29 as can be seen by reference to Fig. 6 of their paper.

Another experimental investigation at a low hypersonic Mach number (4.95) is reported by Julius·(Ref. 30). This test was conducted in the 9-in.-diam blowdown axisymmetric jet at the NASA Langley Research Center; test conditions are given in Table I. The inviscid edge conditions given in Table II for this flow condition are based upon an average of the experimental pressure distribution along the body shown in Fig. 3 of Ref. 30. Because of tunnel effects the model experienced a small decrease in surface pressure over the aft third of the body. The comparison shown in Fig. 23 reveals excellent agreement of results from the present theory and experiment up to the point where the (favorable) pressure gradient tends to reduce the experimental turbulent heat-transfer rate to a value below the theoretical prediction. In the laminar region the experimental data appear high relative to results from the present theory. This is caused by the experimental pressure in the laminar region being higher than the averaged pressure used in the present calculations.

SECTION IV
CONCLUDING SUMMARY

In the above comparisons of experimental results with numerical calculations from the present theory, excellent agreement was obtained in most cases. The present approach appears to yield a reasonably accurate description of transitional heating on slender sharp cones in the Mach number range from 5 to 10 under cold wall conditions. It is important to keep in mind that application of the present theory requires a priori specification of the onset to transition location, X_t, along the body. In the work herein, this location was determined based upon examination of the particular experimental data under investigation. The factor of 2 used to define the end of transition relative to the transition onset distance appears to be adequate for description of sharp cone transitional heat transfer under cold wall conditions in the hypersonic flow regime.

These favorable results indicate that the intermittency factor-eddy viscosity approach coupled with accurate numerical solution of the governing turbulent boundary-layer equations may become a powerful tool in analysis techniques for transitional heating on lifting body configurations. Much work remains to be done in this area as will be discussed in the next section.

SECTION V
FUTURE STUDIES

The continuing need for understanding turbulent boundary layers is more experiments of a so-called microscopic nature, i.e., detailed measurements of the flow field structure performed in parallel with accurate application of the theories now in existence. Above Mach number 5 acceptable detailed measurements of the turbulent boundary-layer structure are almost nonexistent for flows over bodies of aerodynamic interest. Much evidence (see Ref. 40) seems to indicate, at least in the high supersonic or low hypersonic Mach number range, that the general concept of a turbulent mechanism (such as used in the present work) unaffected by the supersonic nature of the mean stream is acceptable. The characteristics of turbulence in both incompressible and compressible flow seem to depend only on the kinematics of the flow. Hence it may well be that one can safely apply the present simple structural hypothesis with confidence in the hypersonic regime; at least the present work indicates that an eddy viscosity approach yields accurate heat-transfer predictions for hypersonic sharp cone transitional and turbulent boundary-layer flows.

25

With respect to extension of the present eddy viscosity-intermittency factor treatment of transition, it is the author's opinion that the following investigations would be of great value in establishing its validity under flow conditions different from the current investigation:

1. Comparison of theory and experiment with respect to heat transfer and skin friction on flat plates in super- sonic and hypersonic flow.

2. Comparison of theory and experiment with respect to heat transfer and skin friction on blunt nosed bodies in supersonic and hypersonic flow.

3. Comparison of theory and experiment with respect to the recovery factor under adiabatic wall conditions in both supersonic and hypersonic flow.

Again detailed measurements of the turbulent boundary-layer structure in each of the above suggested investigations are direly needed in order to strictly assess the theoretical model. Another important result of the above suggested investigations would be the compilation of sufficient experimental data for the body and flow under consideration to permit determination of accurate transition zone descriptive models. There is no reason to believe that the factor of 2 transition zone model used in the present sharp cone investigation will remain valid for, say, a curved flat plate having an adiabatic wall under low supersonic conditions. It may well be that additional experiments must be designed in order to carefully study the transition zone under controlled flow conditions for various body geometries. In any respect, comparison of theory with experiments is the key to understanding the applicability of the current eddy viscosity-intermittency factor prediction technique.

Another area worthy of future work is the application of turbulent transport theory to numerical calculation of transitional boundary-layer structure. A recent paper by Bradshaw, Ferriss, and Atwell (Ref. 41) successfully applies the turbulent energy equation (which is an equation for the rate of change of turbulent intensity along a streamline) to incompressible turbulent flows both with and without pressure gradients. While this method employs several empirical relations, it is more gen- eral than the eddy viscosity boundary-layer approach. Prediction of transition should conceptually be possible using this technique. The only attempt published to date to solve the compressible boundary-layer problem by this approach is that of Bradshaw and Ferriss (Ref. 42) who extended their method for incompressible flow directly to adiabatic flows with $M_\infty \leq 4$. It certainly would be of interest to ascertain if the present intermittency factor-eddy viscosity approach is contained within the basic framework of turbulent transport theory.

The present analysis reported herein covers the first phase of a general analytical investigation having as the end objective accurate numerical prediction techniques for laminar, transitional, and turbulent boundary layers in hypersonic flow along the most windward streamline of arbitrarily shaped bodies at angle of attack. Subsequent reports will document the findings of this ongoing work.

REFERENCES

1. Masaki, M. and Yakura, J. "Transitional Boundary Layer Considerations for the Heating Analyses of Lifting Reentry Vehicles." AIAA Paper 68-1155 (A69-13674) presented at the AIAA Entry Vehicle Systems and Technology Meeting, Williamsburg, Virginia, December 1968.

2. Smith, A. M. O. and Cebeci, T. "Numerical Solution of the Turbulent Boundary-Layer Equations." Douglas Aircraft Division Report 33735, May 1967.

3. Patankar, S. V. and Spalding, D. B. Heat and Mass Transfer in Boundary Layers. CRC Press, Cleveland, Ohio, 1968.

4. Bushnell, D. M. and Beckwith, I. E. "Calculation of Nonequilibrium Hypersonic Turbulent Boundary Layers and Comparisons with Experimental Data." AIAA Paper 69-684 (A69-33474) presented at the AIAA Fluid and Plasma Dynamics Conference, San Francisco, California, June 1969.

5. Herring, H. J. and Mellor, G. L. "A Method of Calculating Compressible Turbulent Boundary Layers." NASA CR-1144, September 1968.

6. Martellucci, A., Rie, H. and Sontowski, J. F. "Evaluation of Several Eddy Viscosity Models through Comparison with Measurements in Hypersonic Flows." AIAA Paper 69-688 (A69-33454) presented at the AIAA Fluid and Plasma Dynamics Conference, San Francisco, California, June 1969.

7. Mayne, A. W., Jr. and Dyer, D. F. "Comparisons of Theory and Experiment for Turbulent Boundary Layers on Simple Shapes at Hypersonic Conditions." Proceedings of the 1970 Heat Transfer and Fluid Mechanics Institute, Stanford University Press, 1970, pp. 168-188.

8. Schubauer, G. B. and Tchen, C. M. "Turbulent Flow." Turbulent Flows and Heat Transfer. Vol. V of High Speed Aerodynamics and Jet Propulsion, C. C. Lin, ed., Princeton Univ. Press, N. J., 1959, pp. 75-119.

9. Dorrance, W. H. Viscous Hypersonic Flow. McGraw-Hill, Inc., 1962.

10. van Driest, E. R. "Turbulent Boundary Layer in Compressible Fluids." J. Aero. Sci., Vol. 18, No. 3, March 1951, pp. 145-160.

11. Escudier, M. P. "The Distribution of the Mixing Length in Turbulent Flows near Walls." Mechanical Eng. Dept. Report TWF/TN/1, Imperial College, London, March 1965.

12. Maise, G. and McDonald, H. "Mixing Length and Kinematic Eddy Viscosity in a Compressible Boundary Layer." (A68-14877) AIAA J., Vol. 6, No. 1, January 1968, pp. 73-80.

13. van Driest, E. R. "On Turbulent Flow near a Wall." J. Aero Sci., Vol. 23, No. 11, November 1956, pp. 1007-1011, 1036.

14. Rotta, J. C. "Recent Developments in Calculation Methods for Turbulent Boundary Layers with Pressure Gradients and Heat Transfer." J. Applied Mech., Vol. 33, No. 2, June 1966, pp. 429-437.

15. Potter, J. L. and Whitfield, J. D. "Effects of Slight Nose Bluntness and Roughness on Boundary-Layer Transition in Supersonic Flows." J. Fluid Mech., Vol. 12, No. 4, April 1962, pp. 501-535.

16. Murphy, J. D. and Rubesin, M. W. "Re-Evaluation of Heat Transfer Data Obtained in Flight Tests of Heat-Sink Shielded Re-Entry Vehicles." J. Spacecraft and Rockets, Vol. 3, No. 1, January 1966, pp. 53-60.

17. Emmons, H. W. "The Laminar-Turbulent Transition in a Boundary Layer - Part I." J. Aero. Sci., Vol. 18, No. 7, July 1951, pp. 490-498.

18. Dhawan, S. and Narasimha, R. "Some Properties of Boundary Layer Flow during the Transition from Laminar to Turbulent Motion." J. Fluid Mech., Vol. 3, No. 4, April 1958, pp. 418-436.

19. Batchelor, G. H. "Note on Free Turbulent Flows with Special Reference to the Two-Dimensional Wake." J. Aero. Sci., Vol. 17, No. 7, July 1950, pp. 441-445.

20. Anon. "Compressible Turbulent Boundary Layers." NASA SP-216, Symposium held at the Langley Research Center, Hampton, Virginia, December 10-11, 1968, pp. 545-564.

21. Spalding, D. B. "Theories of the Turbulent Boundary Layer." Applied Mechanics Reviews, Vol. 20, No. 8, August 1967, pp. 735-740.

22. McDonald, H. "An Assessment of Certain Procedures for Computing the Compressible Turbulent Boundary Layer Development." Paper 6 in "Compressible Turbulent Boundary Layers." NASA SP-216, Symposium held at the Langley Research Center, Hampton, Virginia, December 10-11, 1968, pp. 181-229.

23. Beckwith, I. E. "Recent Advances in Research on Compressible Turbulent Boundary Layers." Paper 18 in "Analytic Methods in Aircraft Aerodynamics." NASA SP-228, Symposium held at Ames Research Center, Moffett Field, California, October 28-30, 1969, pp. 355-411.

24. Smith, A. M. O. "A Decade of Boundary-Layer Research." Applied Mechanics Reviews, Vol. 23, No. 1, January 1970, pp. 1-9.

25. McCauley, W. D., Saydah, A. R., and Bueche, J. F. "Effect of Spherical Roughness on Hypersonic Boundary-Layer Transition." AIAA J., Vol. 4, No. 12, December 1966, pp. 2142-2148.

26. DiCristina, V. "Three-Dimensional Laminar Boundary Layer Transition on a Sharp 8° Cone at Mach No. 10." AIAA Paper 69-12 presented at the AIAA 7th Aerospace Sciences Meeting, New York, January 1969.

27. Sanator, R. J., DeCarlo, J. P. and Torrillo, D. T. "Hypersonic Boundary-Layer Transition Data for a Cold-Wall Slender Cone." AIAA J., Vol. 3, No. 4, April 1965, pp. 758-760.

28. Wilson, D. M. and Fisher, P. D. "Effect of a Highly Cooled Wall on Hypersonic Turbulent Heat Transfer." NOLTR 65-153, June 1966.

29. Wilson, D. M. "Measurements of Hypersonic Turbulent Heat Transfer on a Highly Cooled Cone." NOLTR 67-24, July 1967.

30. Julius, J. D. "Measurements of Pressure and Local Heat Transfer on a 20° Cone at Angles of Attack up to 20° for a Mach Number of 4.95." NASA TN D-179, December 1959.

31. Nagamatsu, H. T. and Sheer, R. E., Jr. "Boundary-Layer Transition on a 10° Cone in Hypersonic Flow." AIAA J., Vol. 3, No. 11, November 1965, pp. 2054-2061.

32. Everhart, P. E. and Hamilton, H. H. "Experimental Investigation of Boundary-Layer Transition on a Cooled 7.5° Total-Angle Cone at Mach 10." NASA TN D-4188, October 1967.

33. Stetson, K. F. and Rushton, G. H. "Shock Tunnel Investigation of Boundary-Layer Transition at M = 5.5." AIAA J., Vol. 5, No. 5, May 1967, pp. 899-906.

34. Sims, J. L. "Tables for Supersonic Flow Around Right Circular Cones at Zero Angle of Attack." NASA SP-3004, 1964.

35. Maddalon, D. V. and Henderson, A., Jr. "Boundary-Layer Transition on Sharp Cones at Hypersonic Mach Numbers." AIAA J., Vol. 6, No. 3, March 1968, pp. 424-431.

36. Potter, J. L. and Whitfield, J. D. "Effects of Unit Reynolds Number, Nose Bluntness, and Roughness on Boundary Layer Transition." AEDC-TR-60-5 (AD234478), March 1960.

37. Wallace, J. E. "Hypersonic Turbulent Boundary-Layer Measurements Using an Electron Beam." CAL AN-2112-Y-1, August 1968.

38. Wallace, J. E. "Hypersonic Turbulent Boundary-Layer Studies at Cold Wall Conditions." Proceedings of the 1967 Heat Transfer and Fluid Mechanics Institute, Stanford University Press, 1967, pp. 427-451.

39. Pinckney, S. Z. "Static-Temperature Distribution in a Flat-Plate Compressible Turbulent Boundary Layer with Heat Transfer." NASA TN D-4611, June 1968.

40. Harvey, W. D., Bushnell, D. M. and Beckwith, I. E. "Fluctuating Properties of Turbulent Boundary Layers for Mach Numbers up to 9." NASA TN D-5496, October 1969.

41. Bradshaw, P., Ferriss, D. H. and Atwell, N. P. "Calculation of Boundary-Layer Development Using the Turbulent Energy Equation." J. Fluid Mech., Vol. 28, No. 3, May 1967, pp. 593-616.

42. Bradshaw, P. and Ferriss, D. H. "Calculation of Boundary-Layer Development Using the Turbulent Energy Equation. II - Compressible Flow on Adiabatic Walls." NPL Aero Rep. 1217, November 1966.

43. Davis, R. T. "The Hypersonic Fully Viscous Shock-Layer Problem." Sandia Corporation Report SC-RR-68-840, December 1968.

44. Blottner, F. G. "Finite Difference Methods of Solution of the Boundary-Layer Equations." AIAA J., Vol. 8, No. 2, February 1970, pp. 193-205.

45. Richtmyer, R. D. and Morton, K. W. Difference Methods for Initial-Value Problems, Second Edition. Interscience Publishers, New York, 1967.

46. Flügge-Lotz, I. and Blottner, F. G. "Computation of the Compressible Laminar Boundary-Layer Flow Including Displacement Thickness Interaction Using Finite-Difference Methods." Stanford University Division of Engineering Mechanics Report No. 131, Stanford, California, January 1962.

47. Adams, J. C., Jr. "Thin Viscous Shock Layer Analysis of Blunt Body Stagnation-Point Air Ionization." (A69-41917) AIAA J., Vol. 7, No. 7, July 1969, pp. 1396-1398.

APPENDIXES

∞

L

x

δ_v

r_b

r_b

v

u

y

$\mathcal{C}_L$
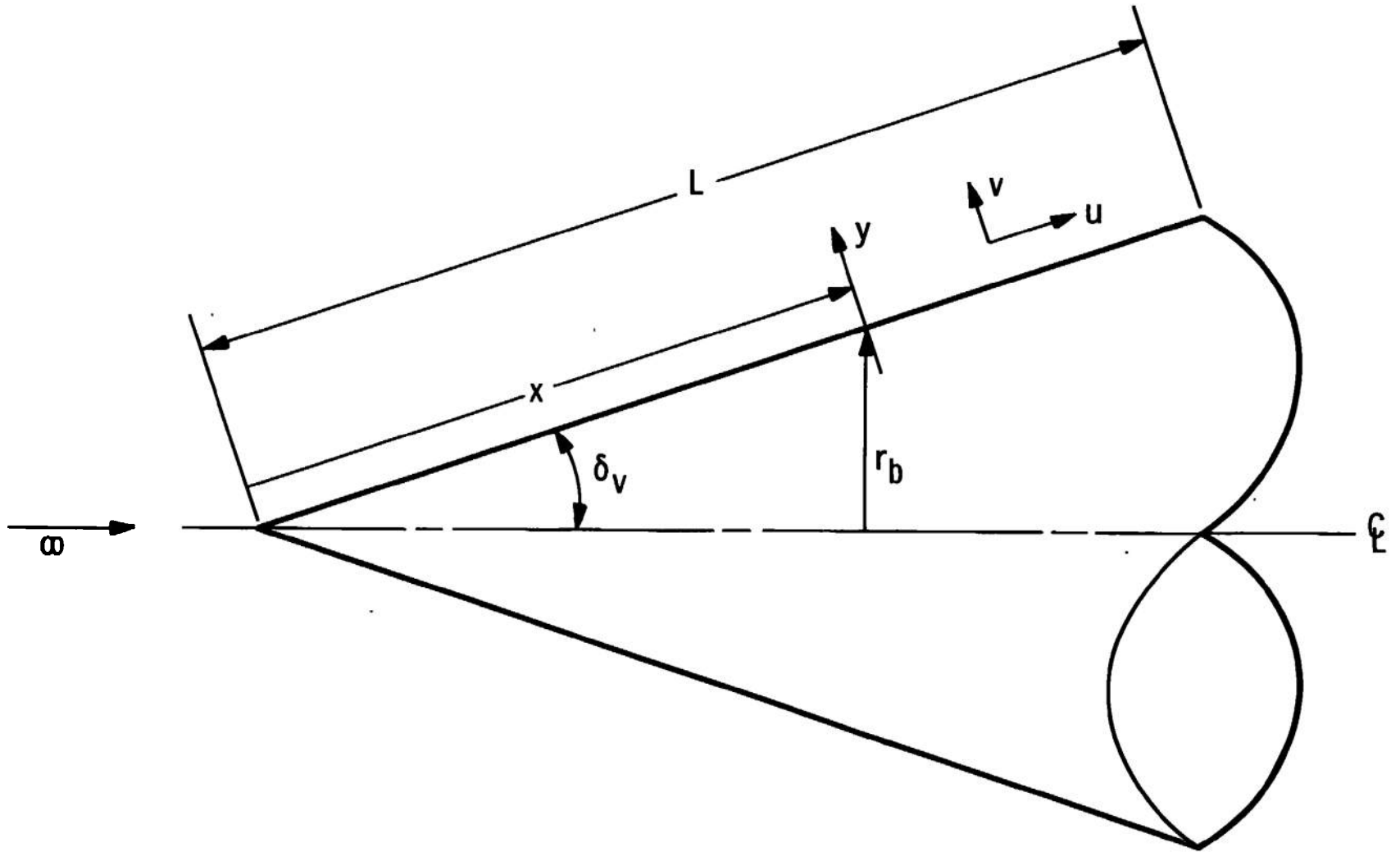
Fig. 1 Sharp Cone Geometry
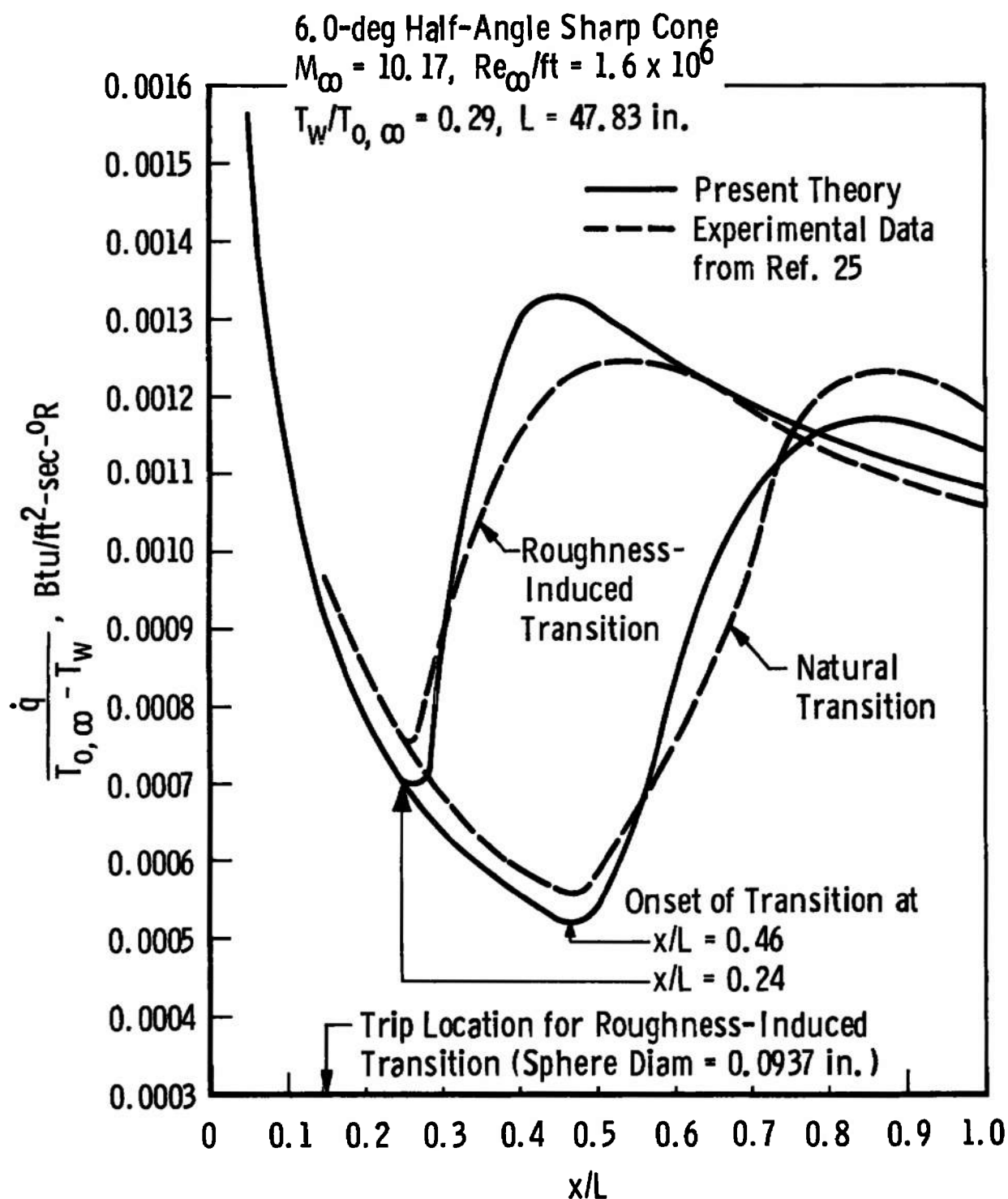
Fig. 2 Comparison of Present Results with Experimental Data
of McCauley, Saydah, and Bueche (Ref. 25)
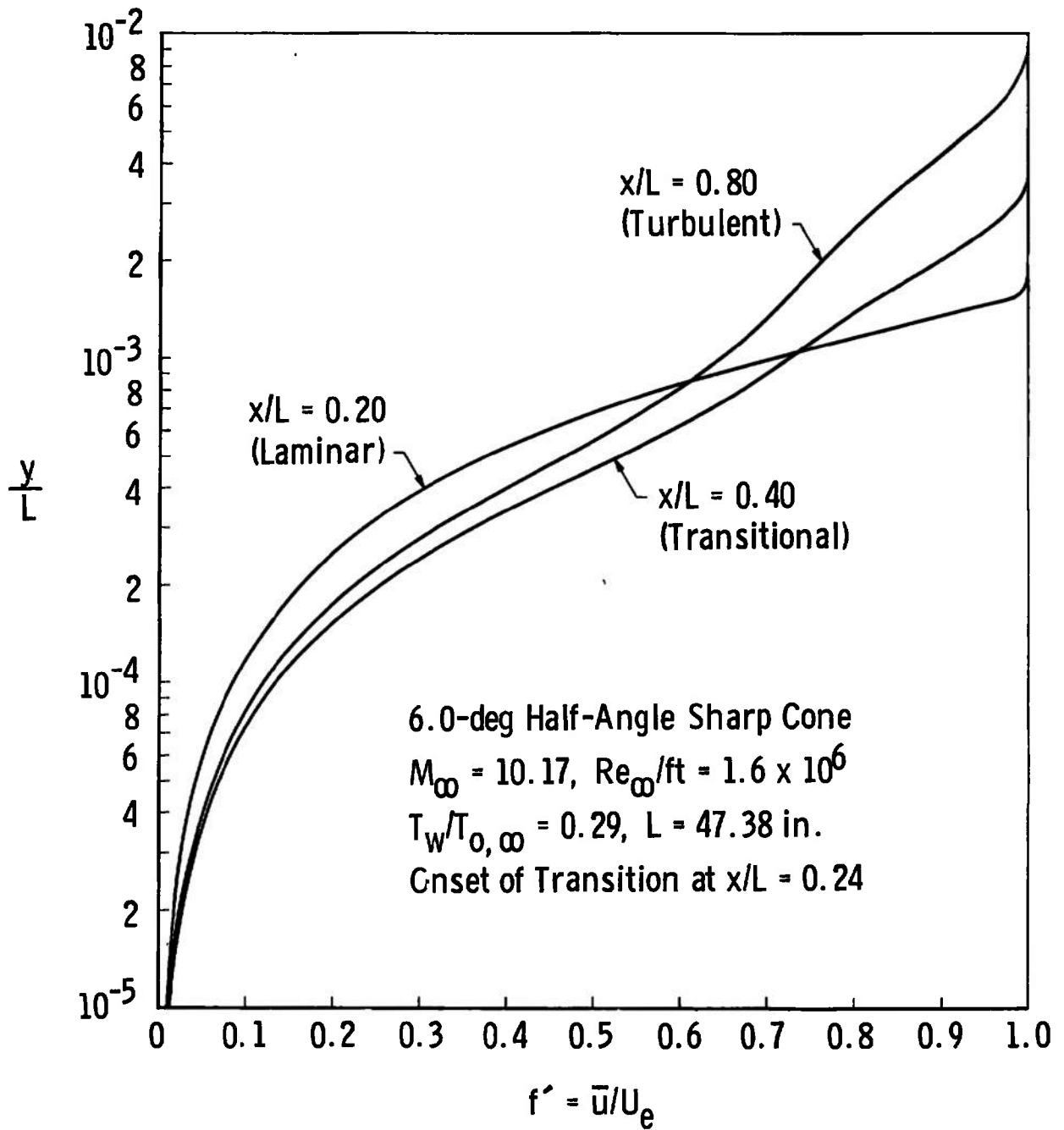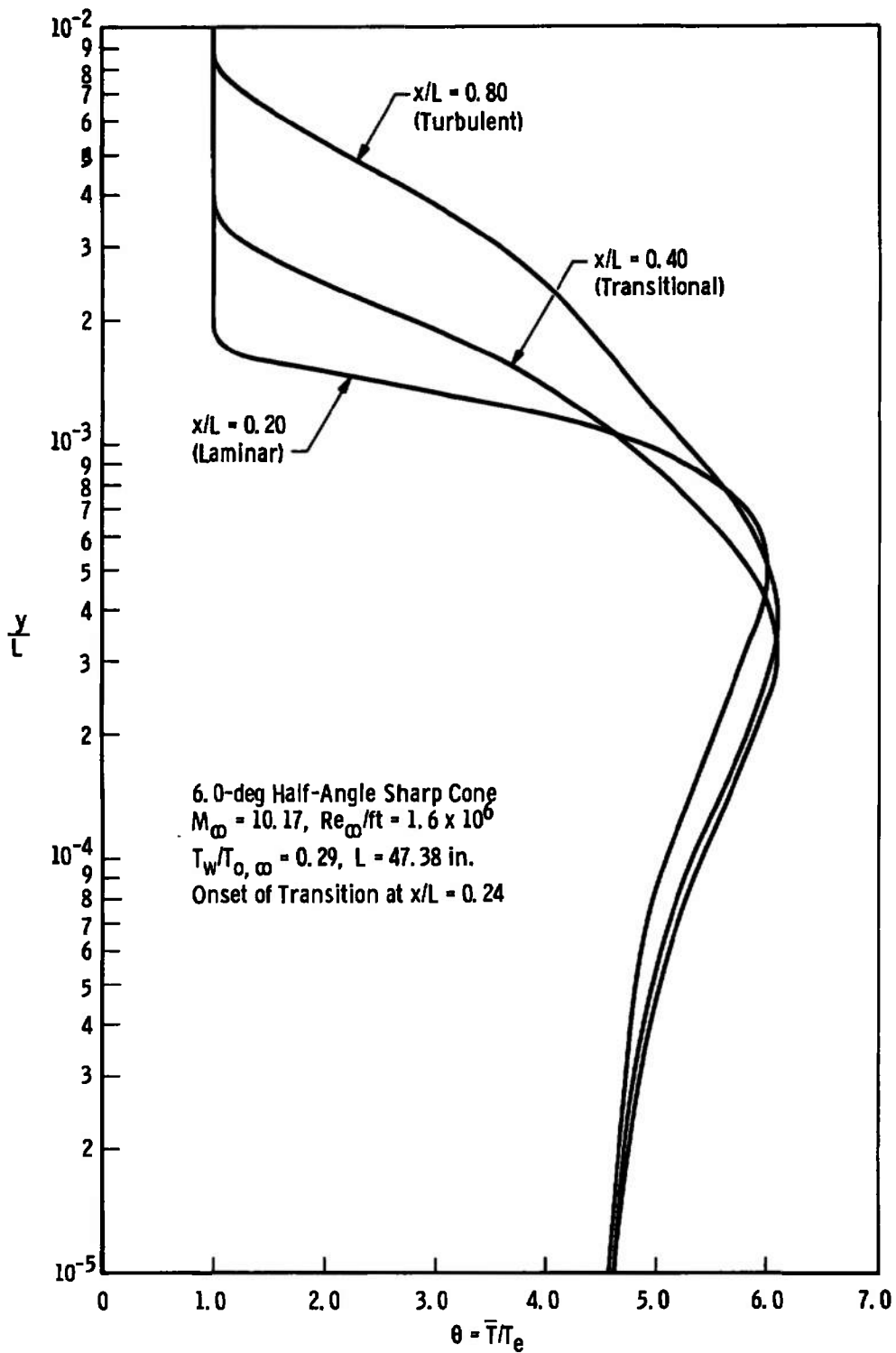
Fig. 3 Calculated Velocity Profiles

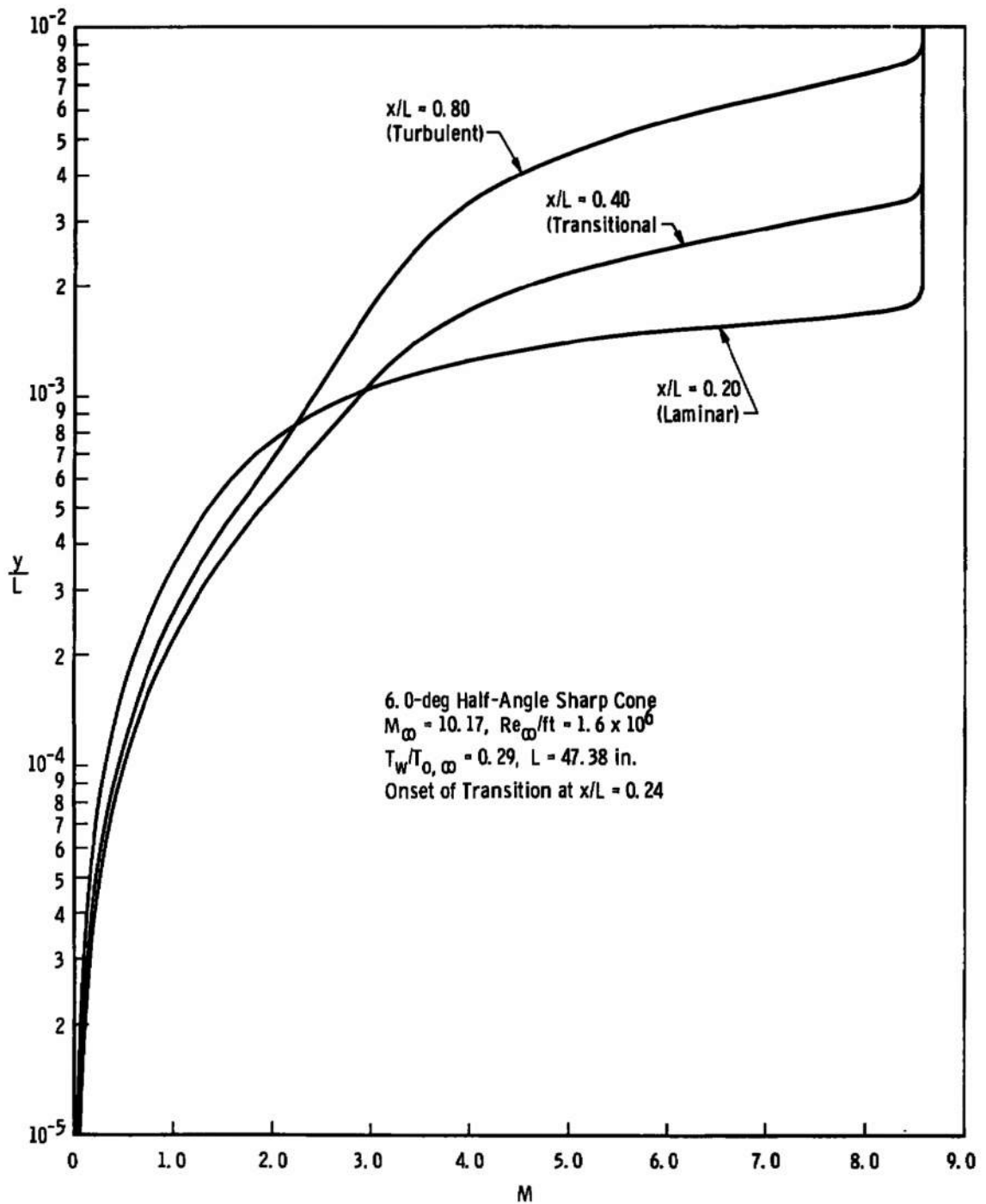Fig. 4 Calculated Static Temperature Profiles

Fig. 5 Calculated Mach Number Profiles

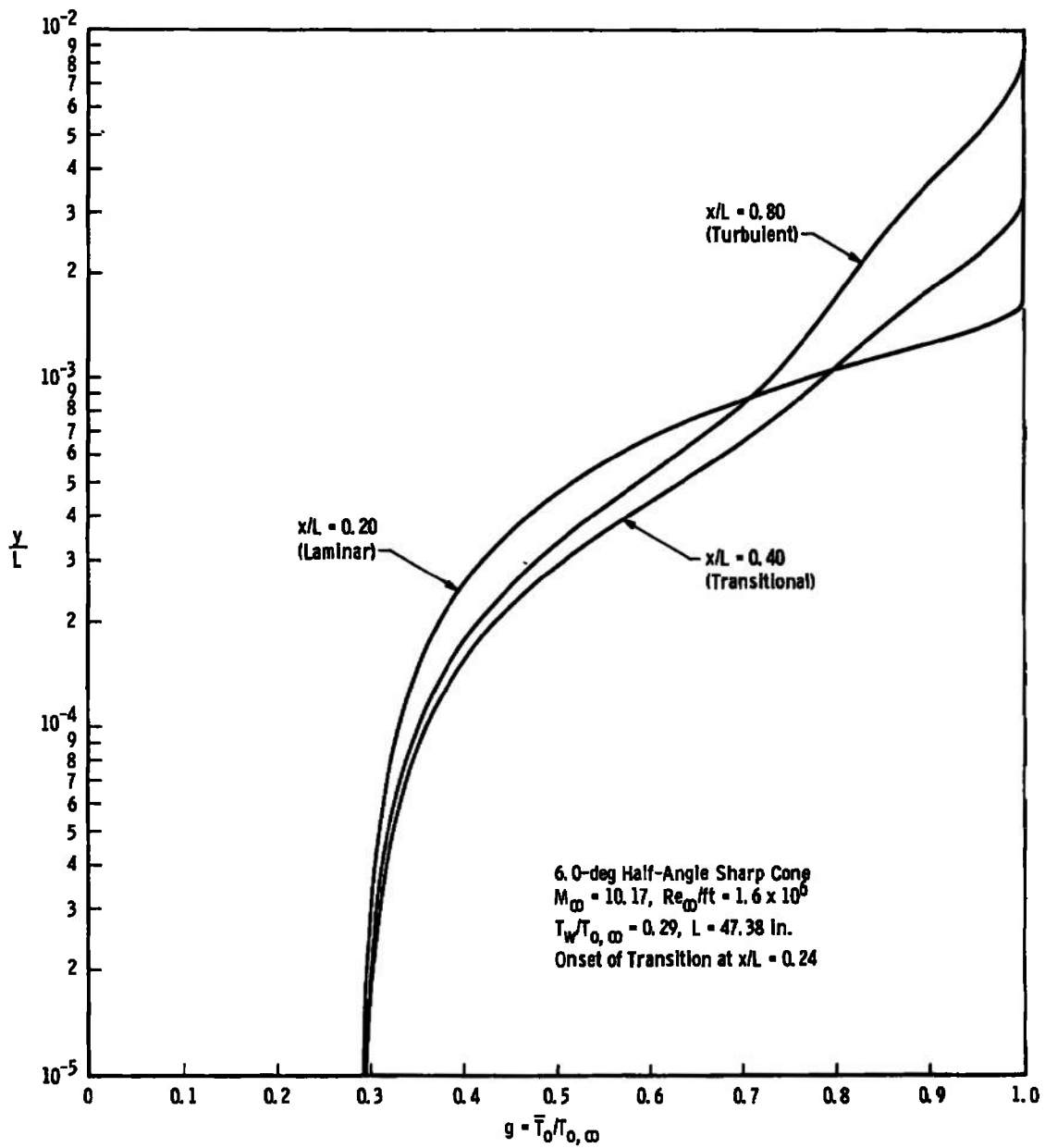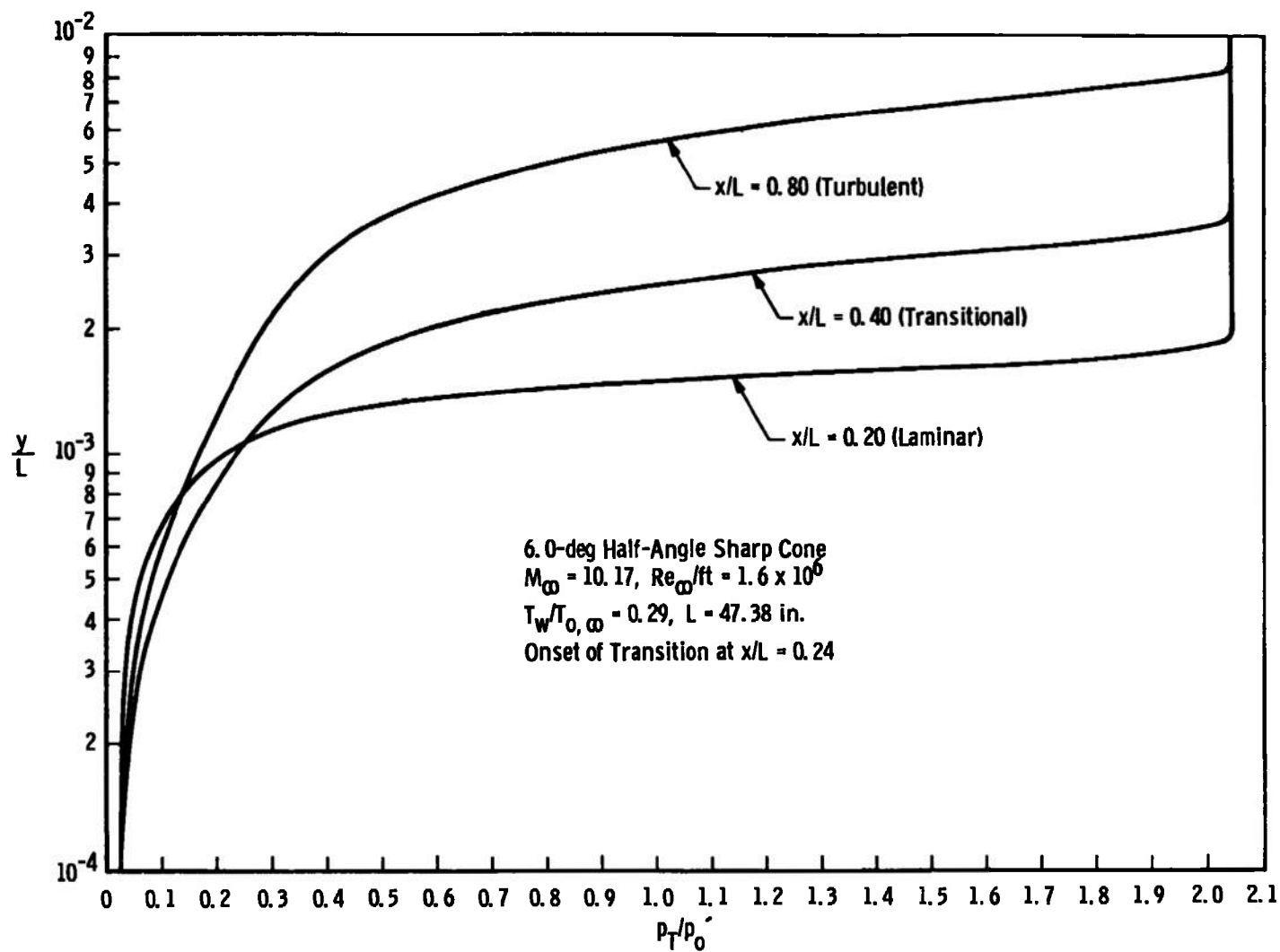Fig. 6 Calculated Stagnation Temperature Profiles

6. 0-deg Half-Angle Sharp Cone
$M_\infty = 10.17$, $Re_\infty/ft = 1.6 \times 10^6$
$T_w/T_{0,\infty} = 0.29$, L = 47.38 in.
Onset of Transition at x/L = 0.24
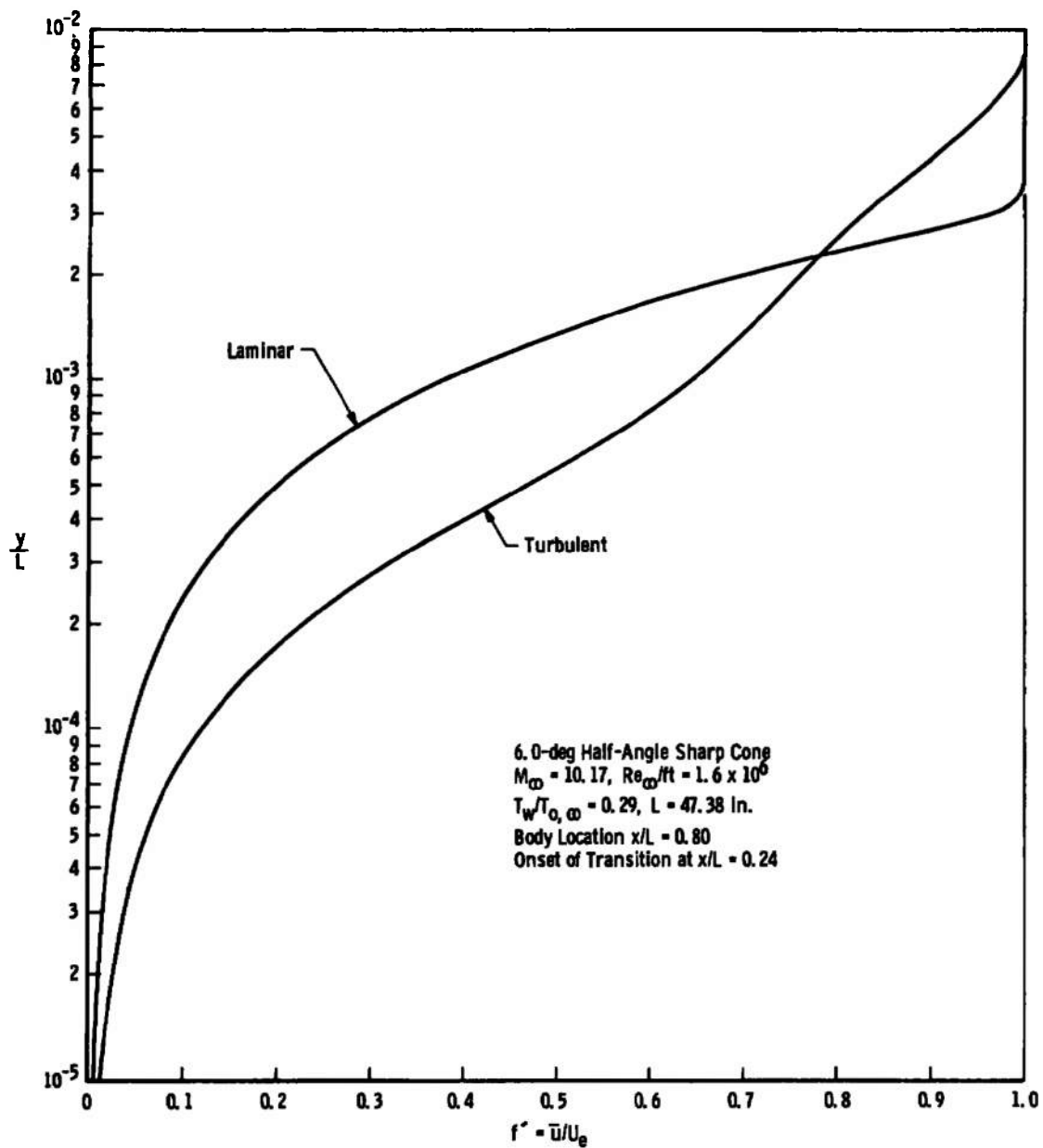
Fig. 7 Calculated Pitot Pressure Profiles

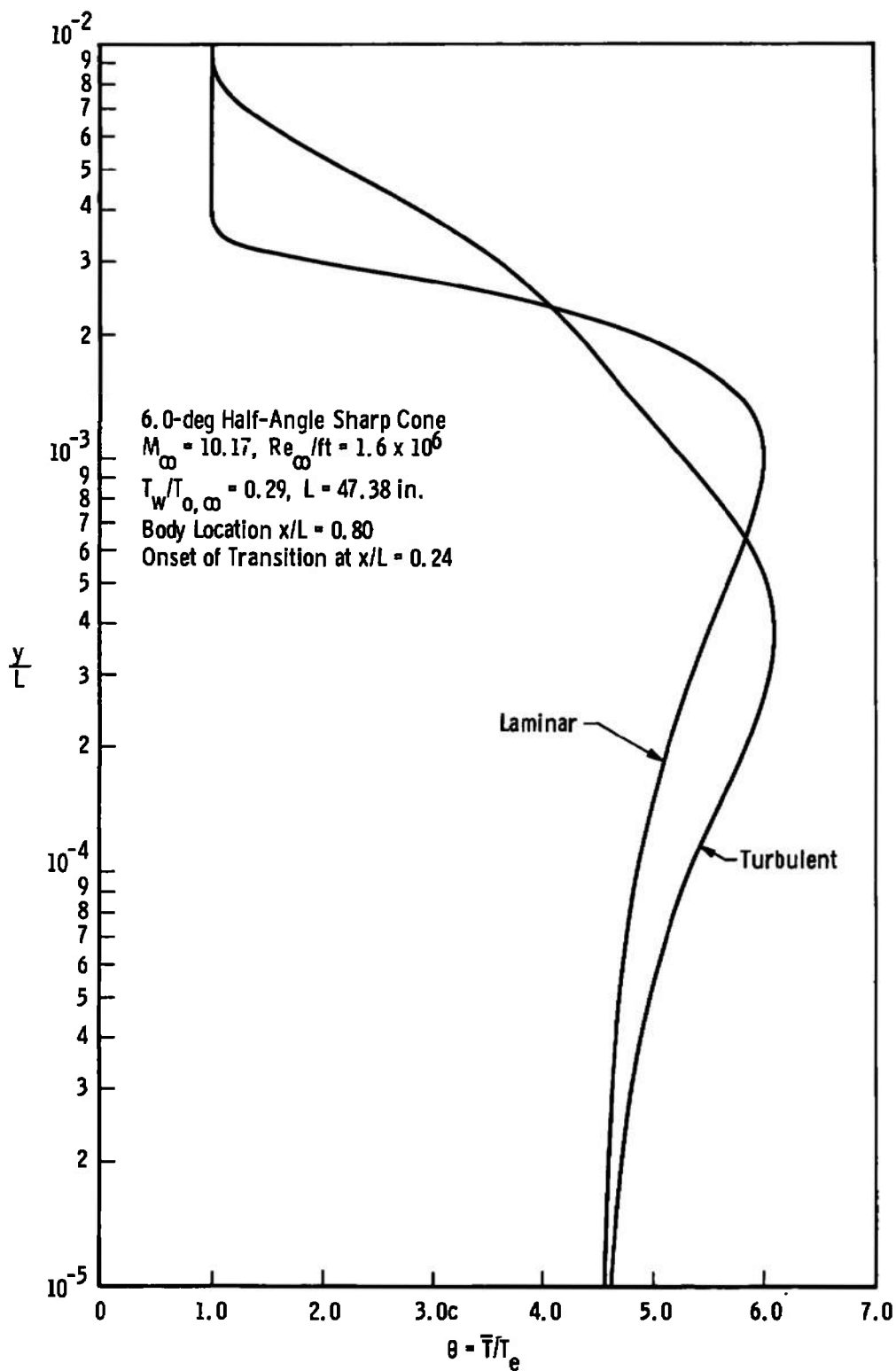Fig. 8 Comparison of Laminar and Fully Turbulent Velocity Profiles

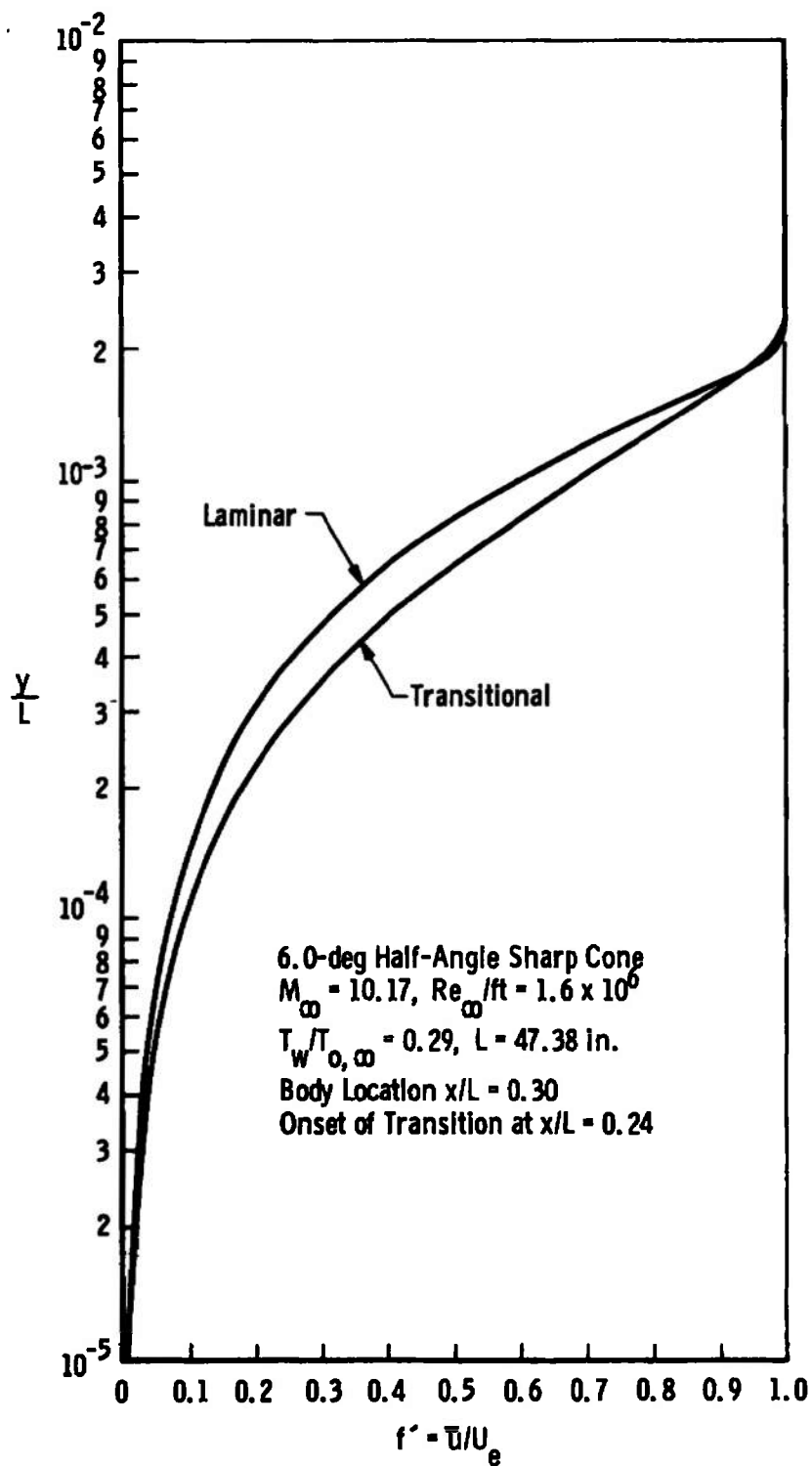Fig. 9 Comparison of Laminar and Fully Turbulent Static Temperature Profiles

Fig. 10 Comparison of Laminar and Transitional Velocity Profiles

6.0-deg Half-Angle Sharp Cone
$M_\infty = 10.17$, $Re_\infty/ft = 1.6 \times 10^6$
$T_w/T_{0,\infty} = 0.29$, $L = 47.38$ in.
Body Location $x/L = 0.30$
Onset of Transition at $x/L = 0.24$

Laminar

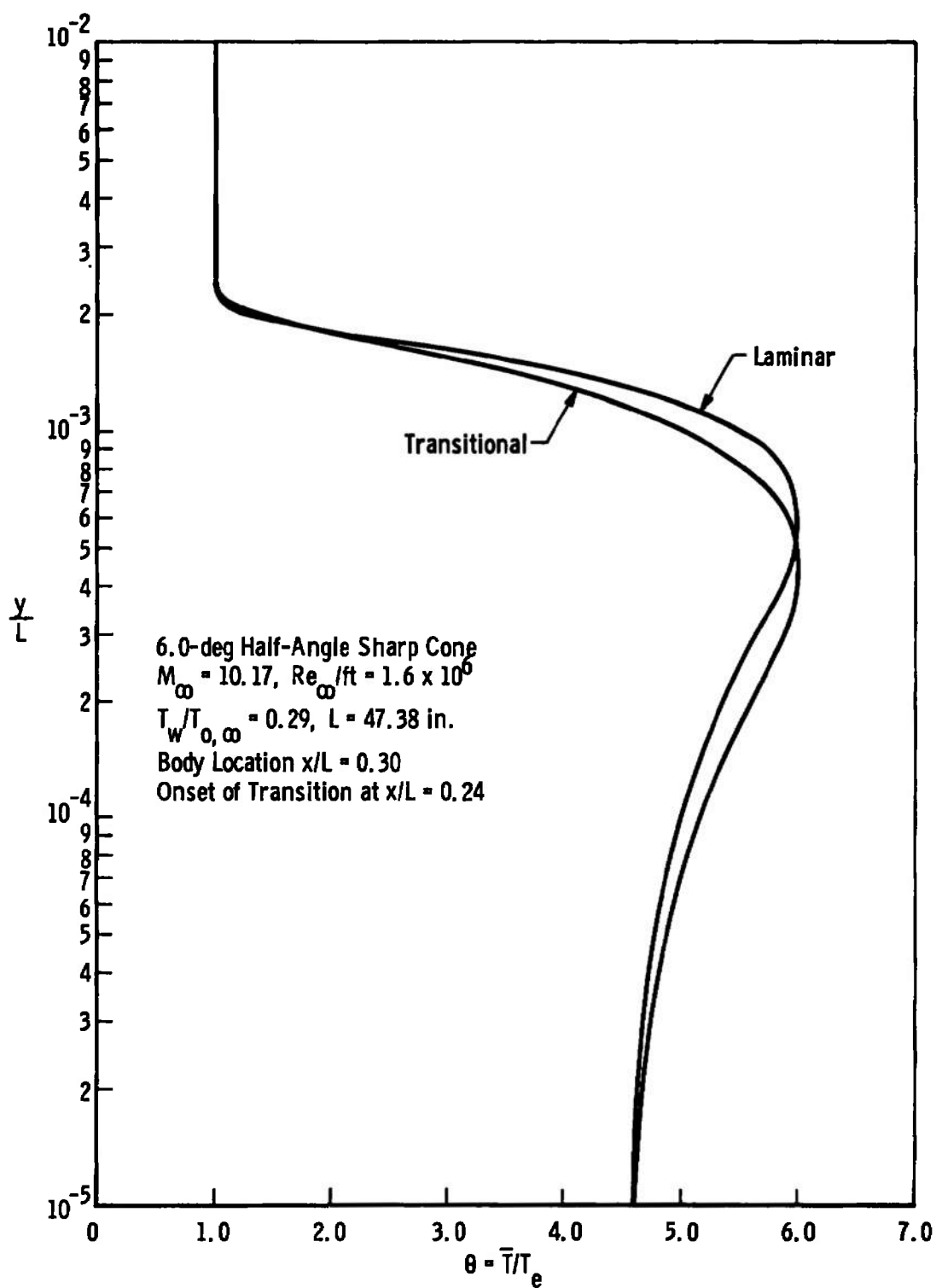Transitional

$\theta = \overline{T}/T_e$

Fig. 11 Comparison of Laminar and Transitional Static Temperature Profiles
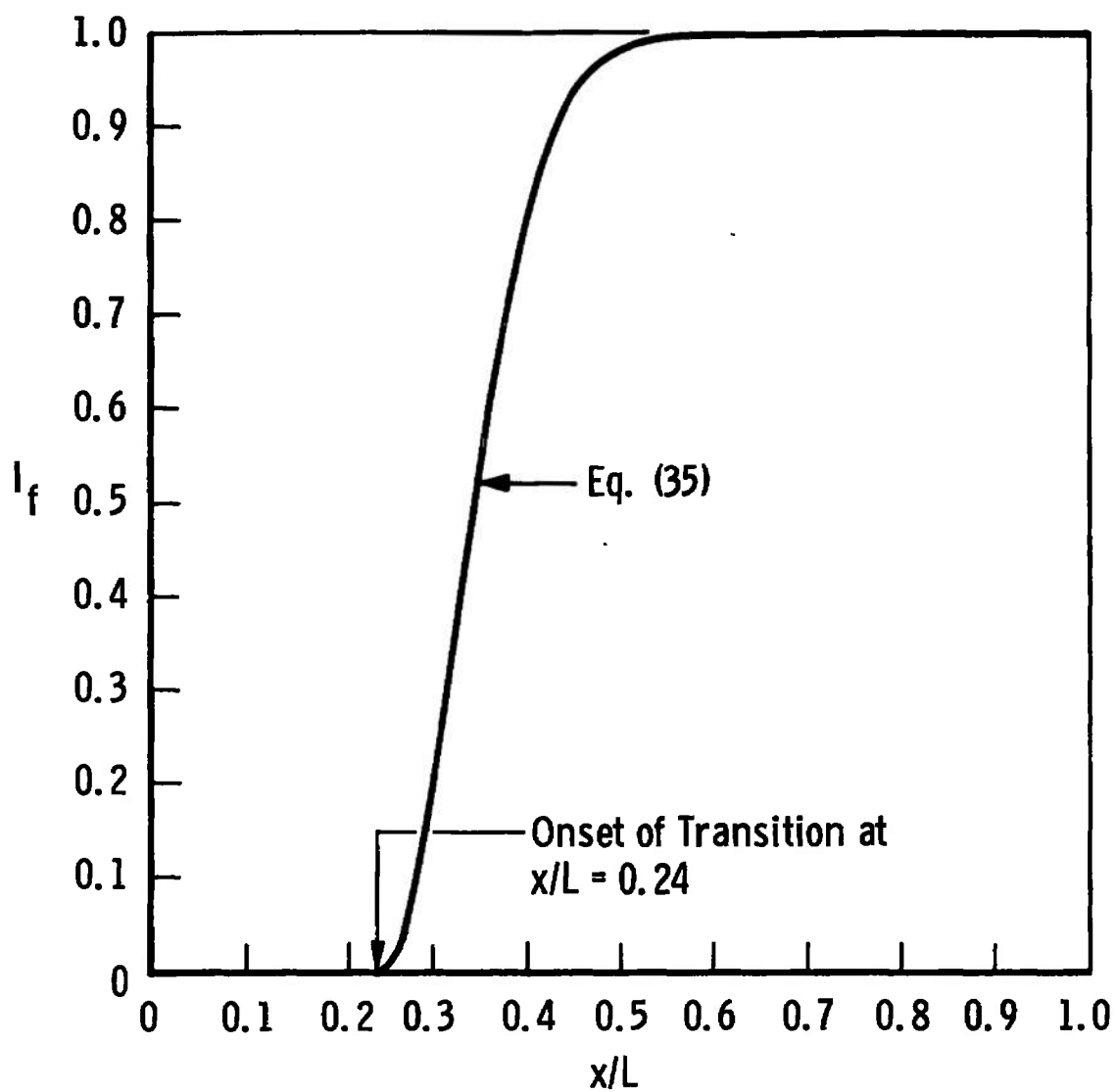
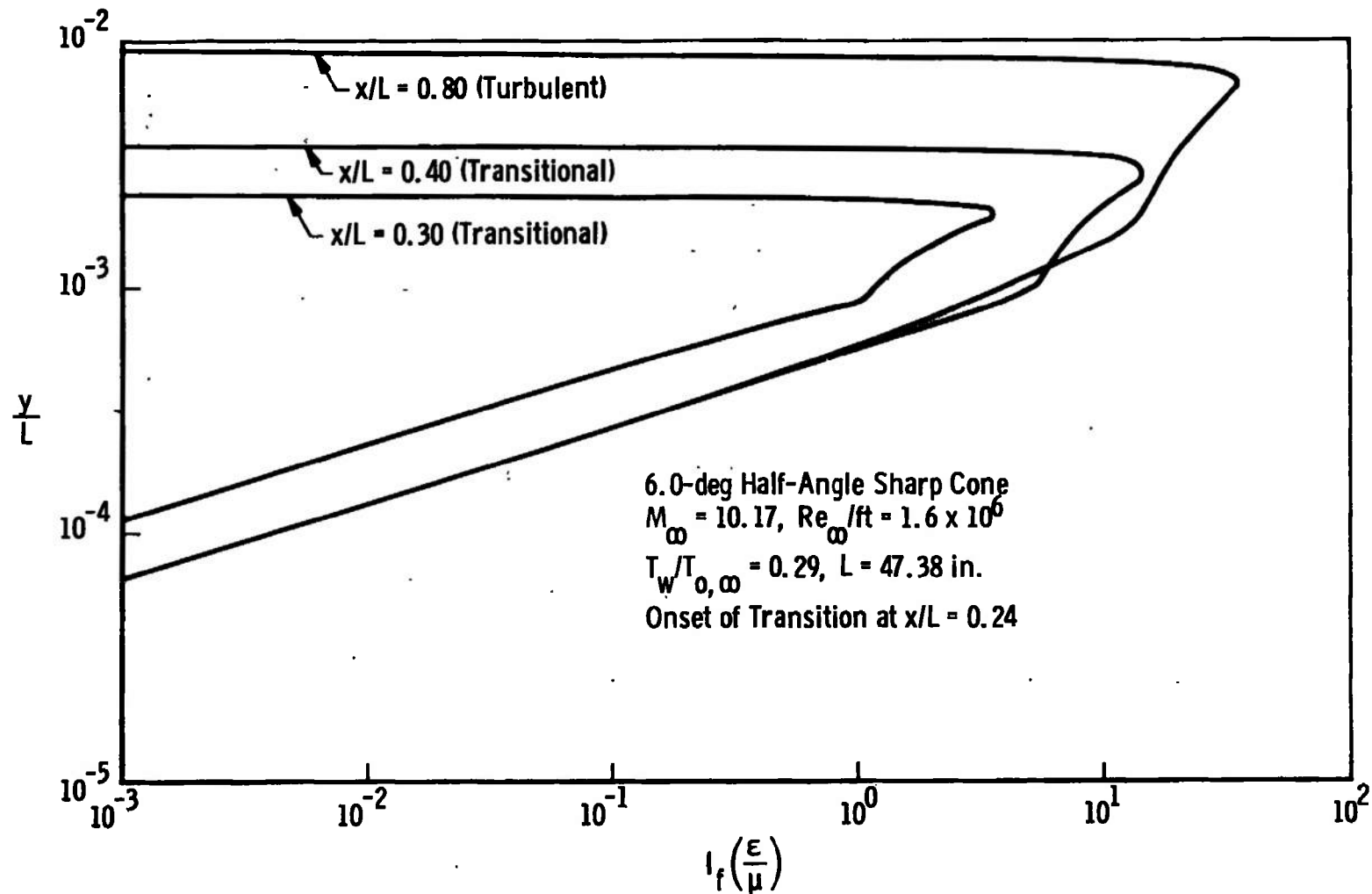Fig. 12 Intermittency Factor Variation along Body

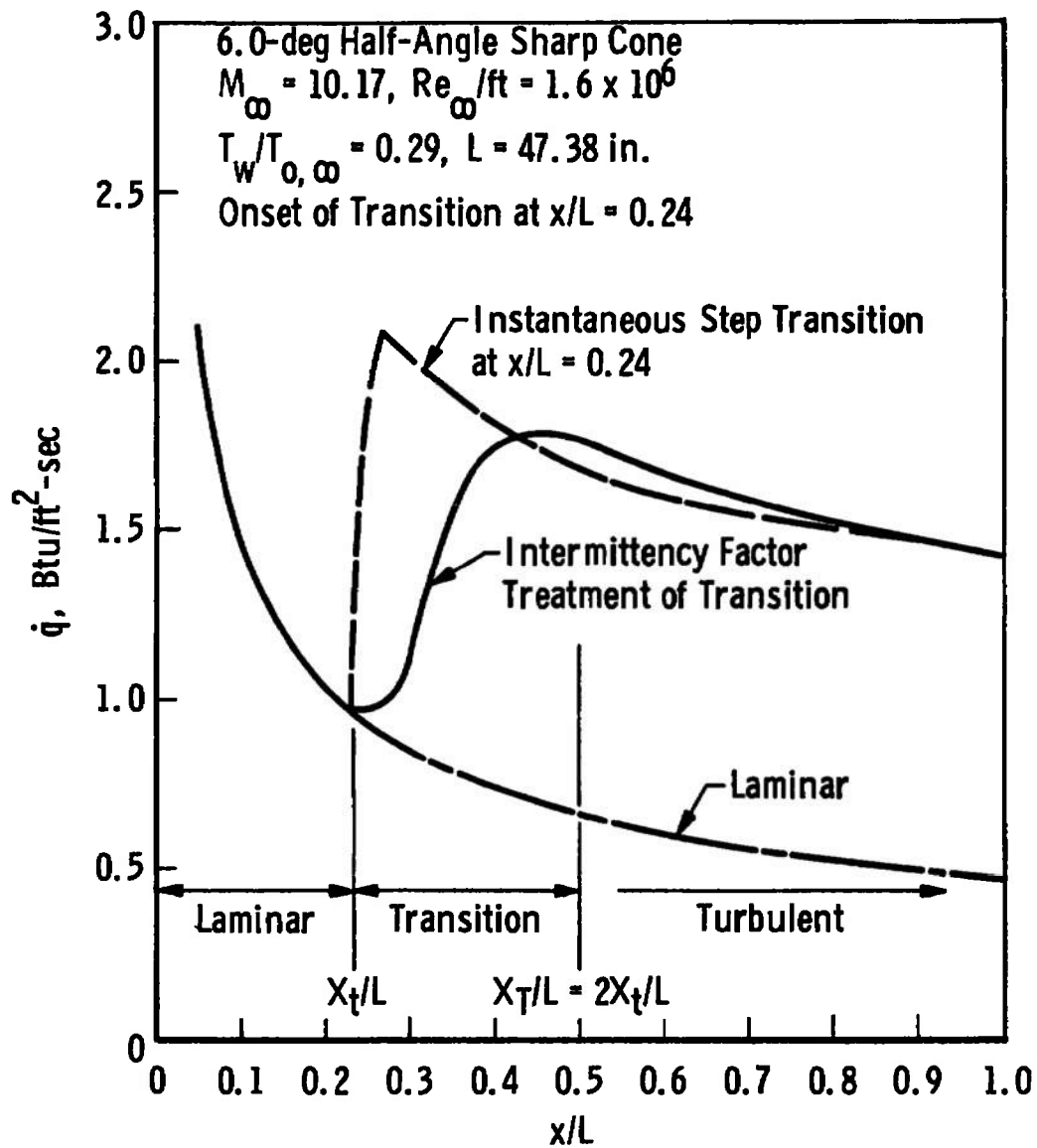Fig. 13 Eddy Viscosity Distributions at Various Body Locations

Fig. 14 Effects of Various Transition Zone Models on Heat-Transfer-Rate Distribution
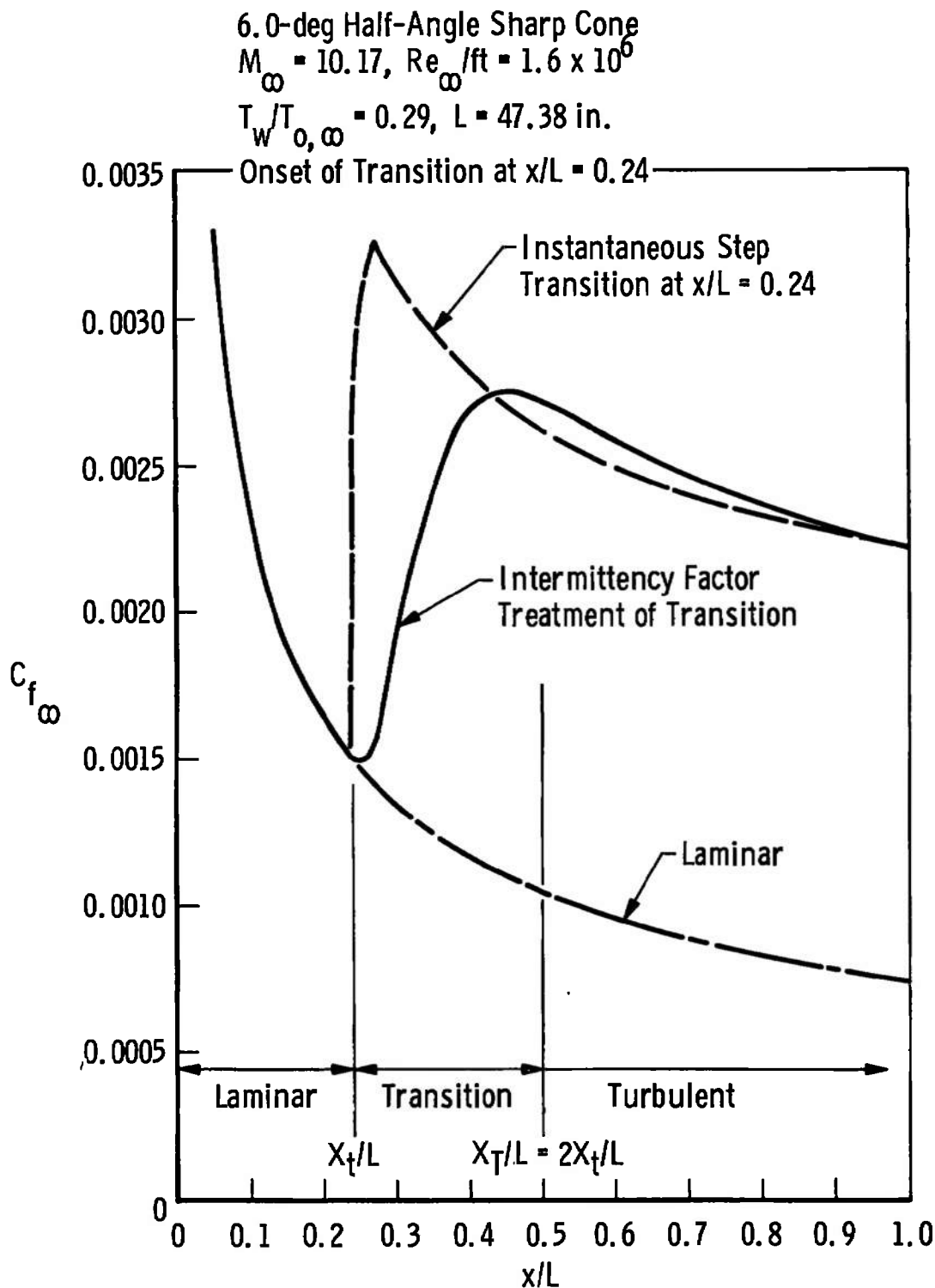
Fig. 15 Effects of Various Transitional Zone Models on Skin Friction Coefficient Distribution
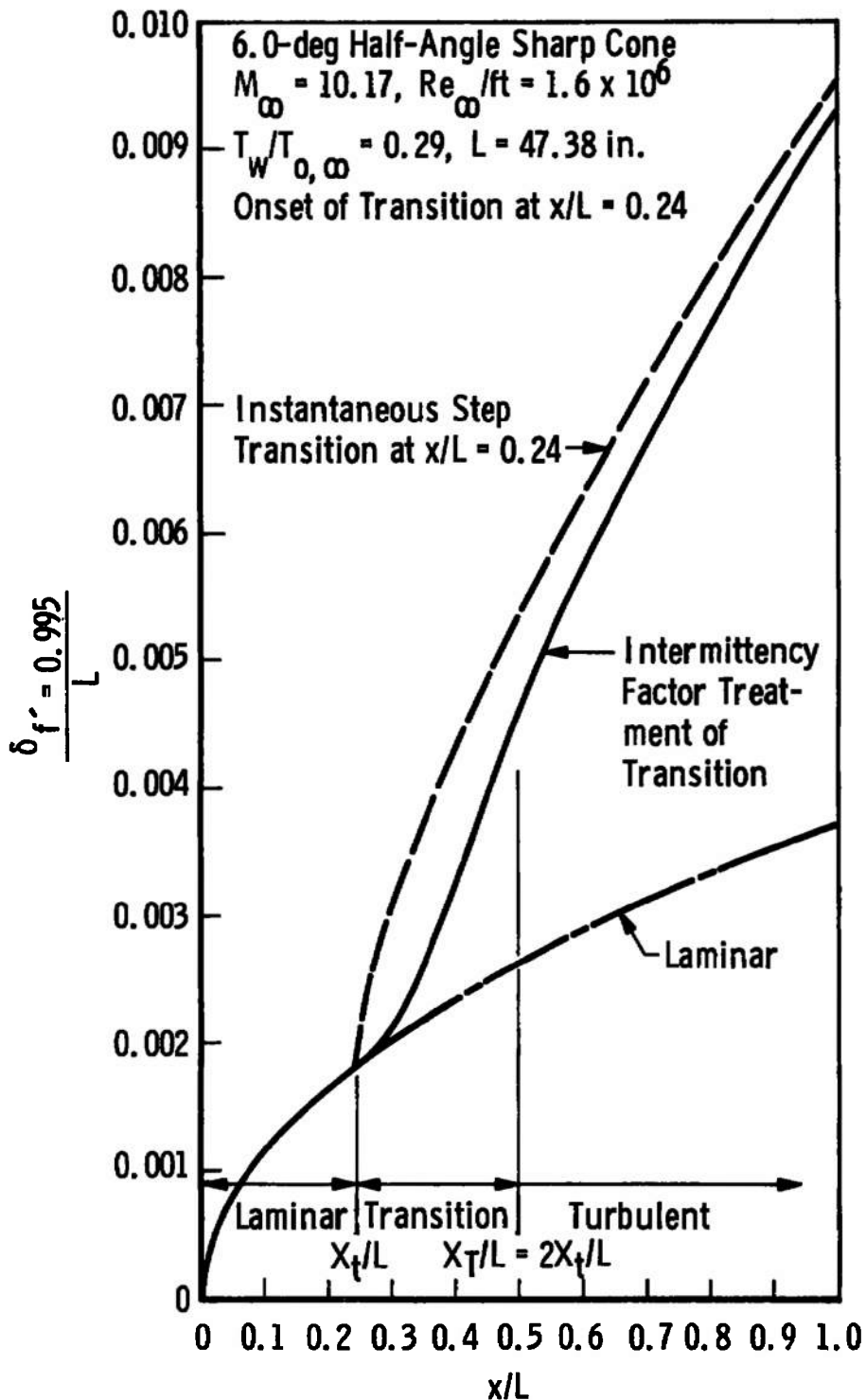
Fig. 16 Effects of Various Transition Zone Models on Boundary-Layer Thickness
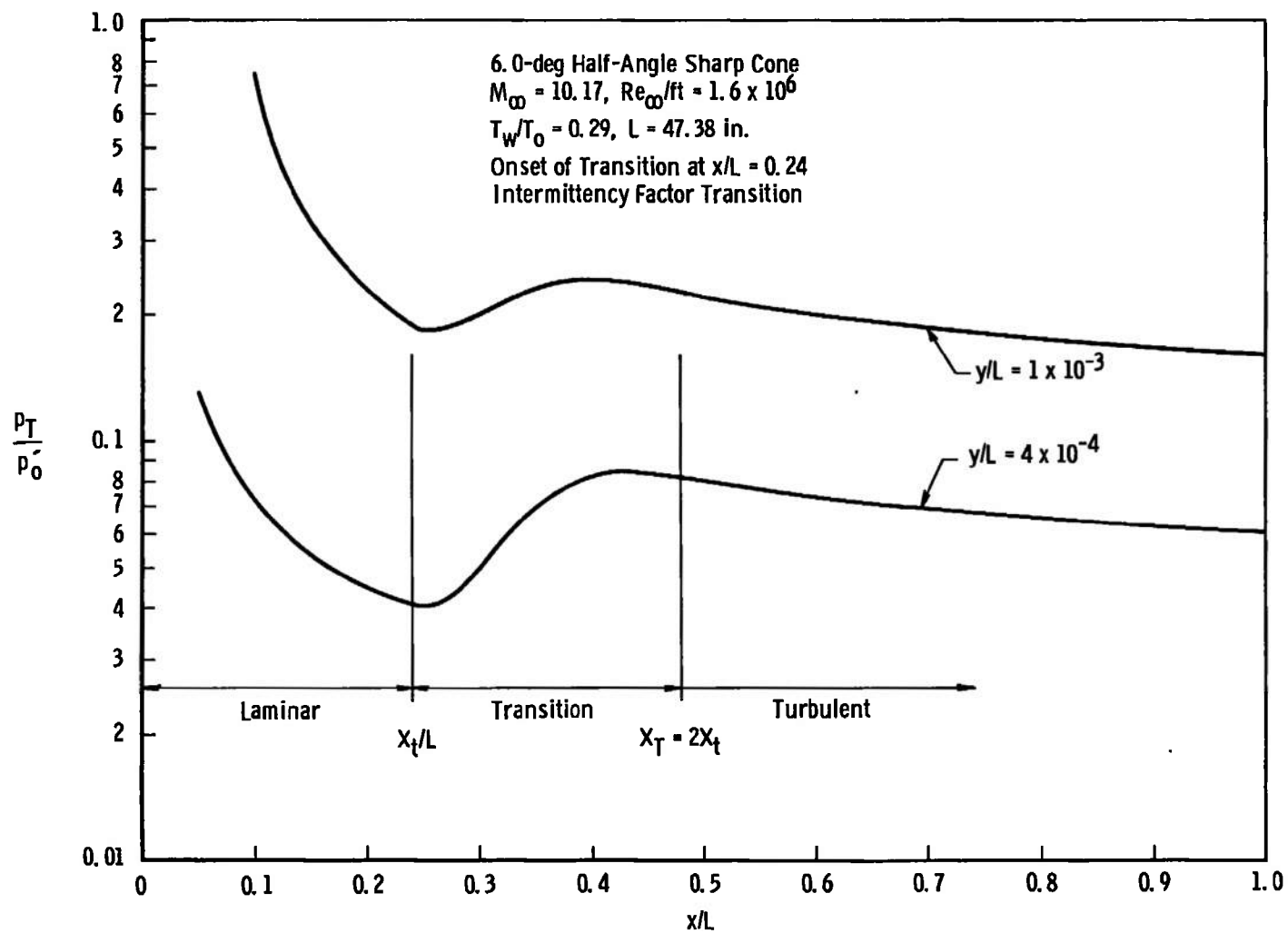
Fig. 17 Fixed Normal Location Pitot Pressure Distribution along Body

6.0-deg Half-Angle Sharp Cone
$M_\infty = 10.17$, $Re_\infty/ft = 1.6 \times 10^6$
$T_w/T_{0,\infty} = 0.29$, $L = 47.38$ in.

Crocco Relation
$g = g_w + f'(1 - g_w)$

Present Theory for Laminar, Transitional, and Turbulent Flow
$0.10 \leq x/L \leq 1.0$
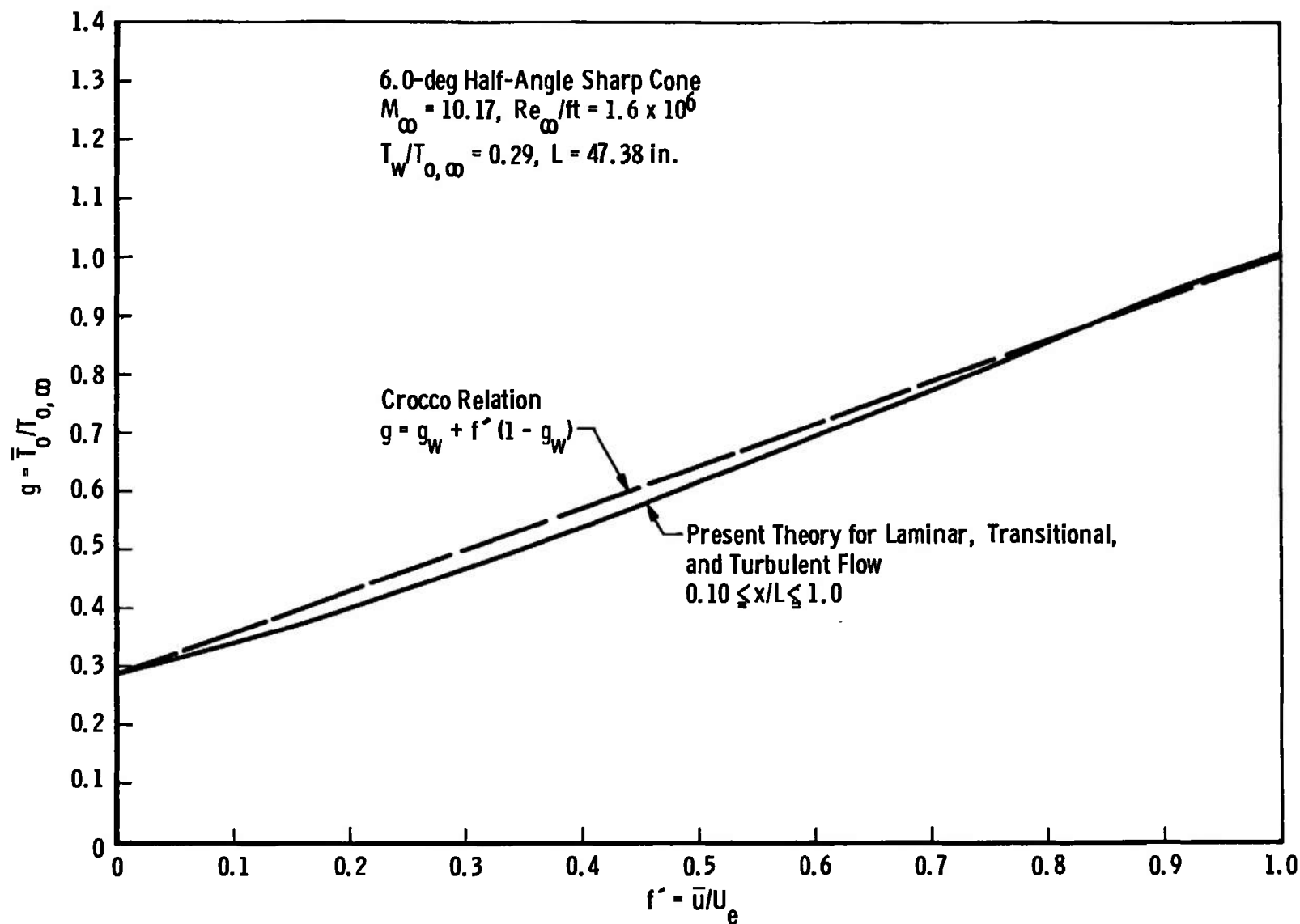
Fig. 18 Comparison of Present Results Relative to Crocco Relation
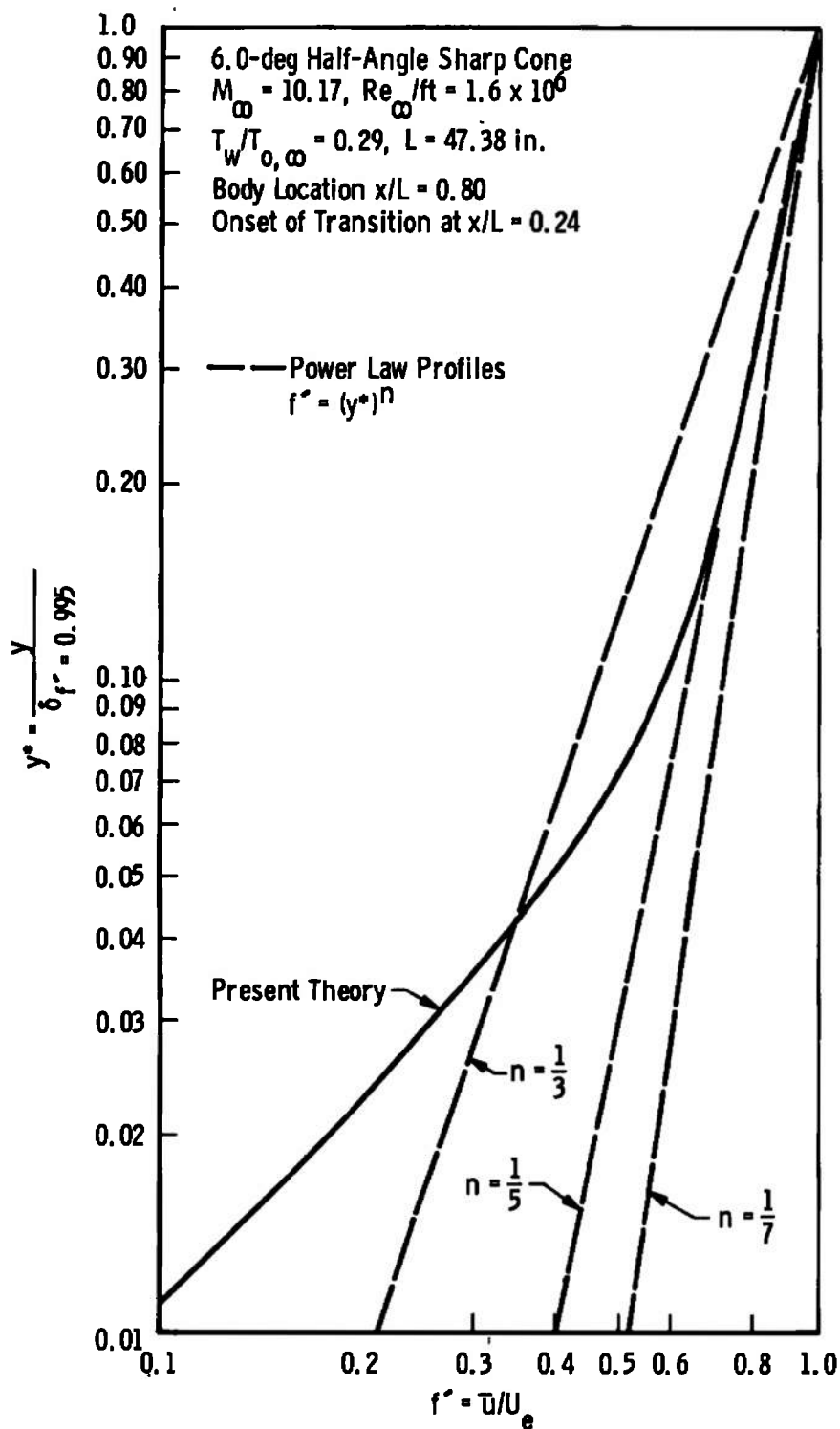
Fig. 19 Comparison of Present Velocity Profile with Several
Power-Law Profiles
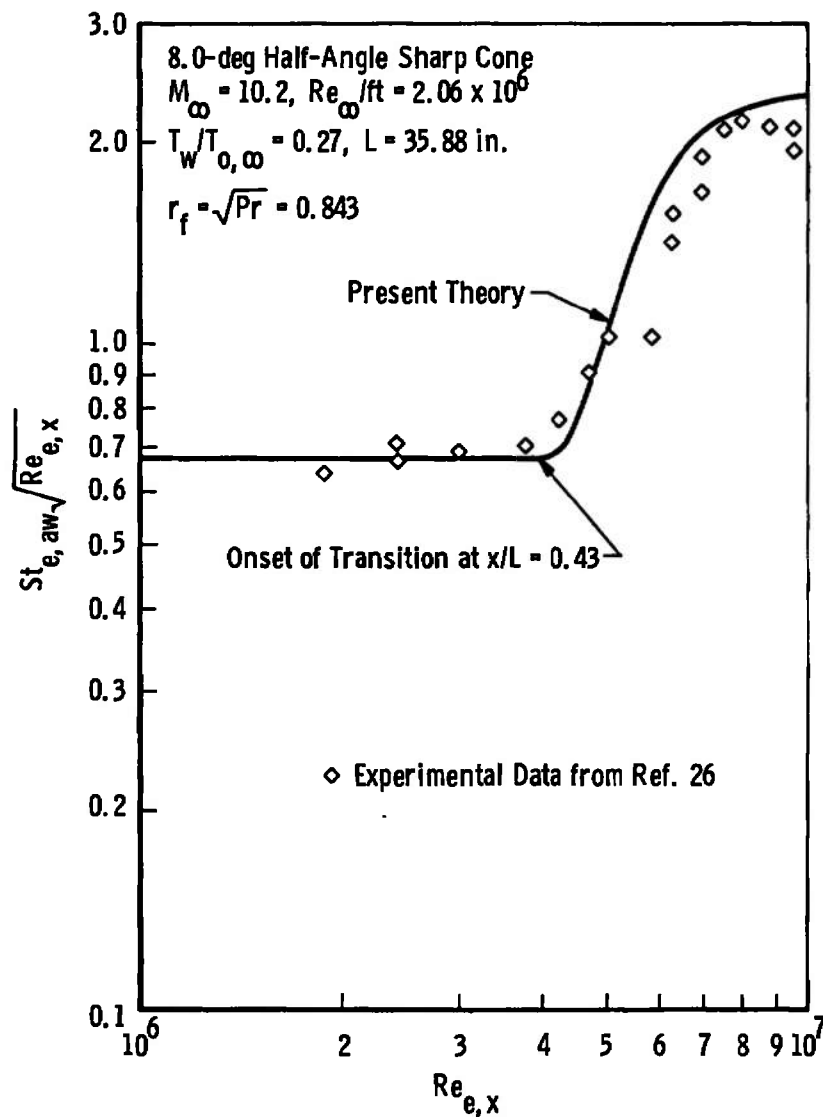
Fig. 20 Comparison of Present Results with Experimental Data
of DiCristina (Ref. 26)

Fig. 21 Comparison of Present Results with Experimental Data of Sanator,
DeCarlo, and Torrillo (Ref. 27)

Fig. 22 Comparison of Present Results with Experimental Data of Wilson
and Fisher (Ref. 28) and Wilson (Ref. 29)
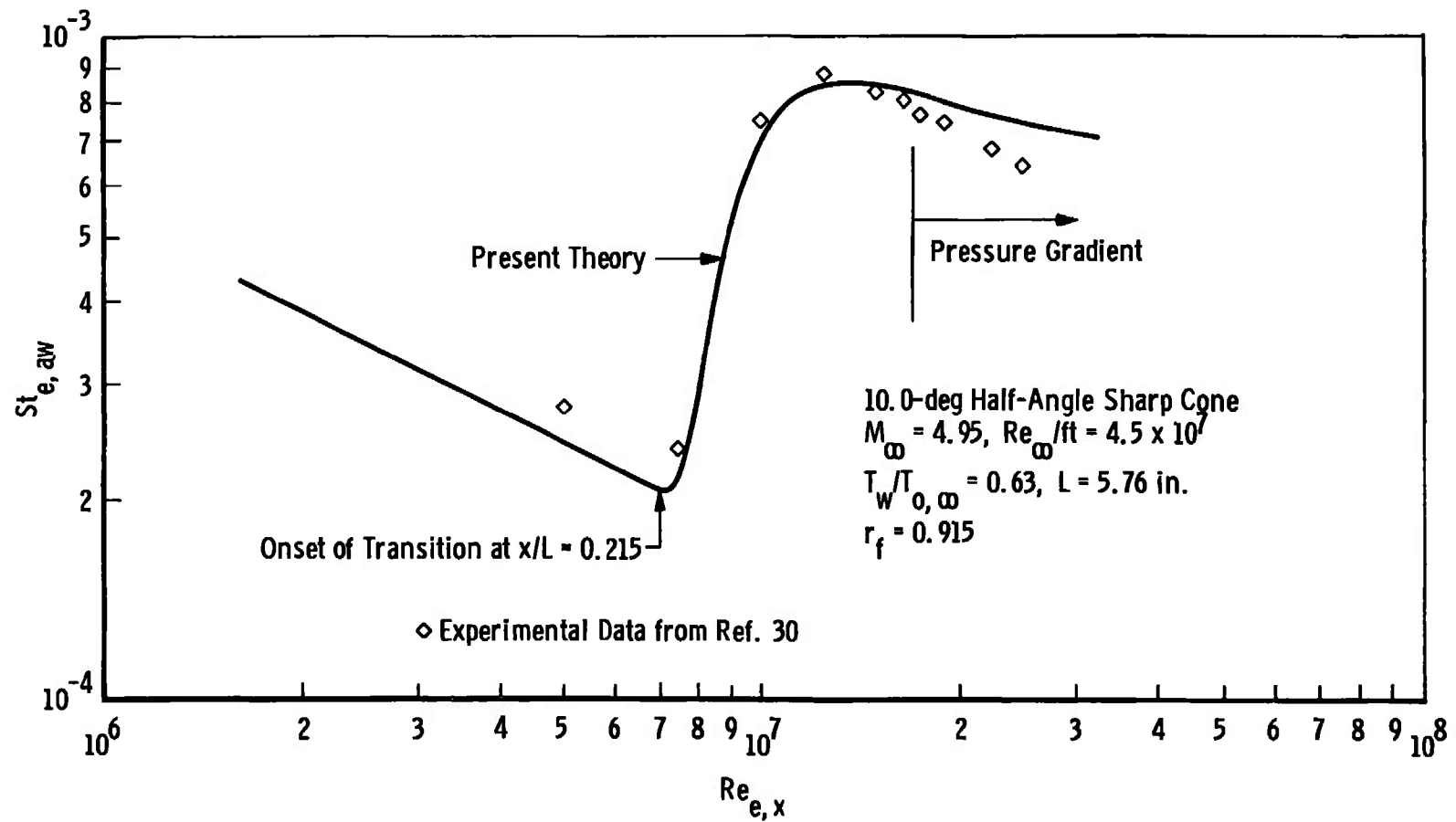
Fig. 23 Comparison of Present Results with Experimental Data of Julius (Ref. 30)

TABLE I
SUMMARY OF EXPERIMENTAL DATA USED IN COMPARISONS

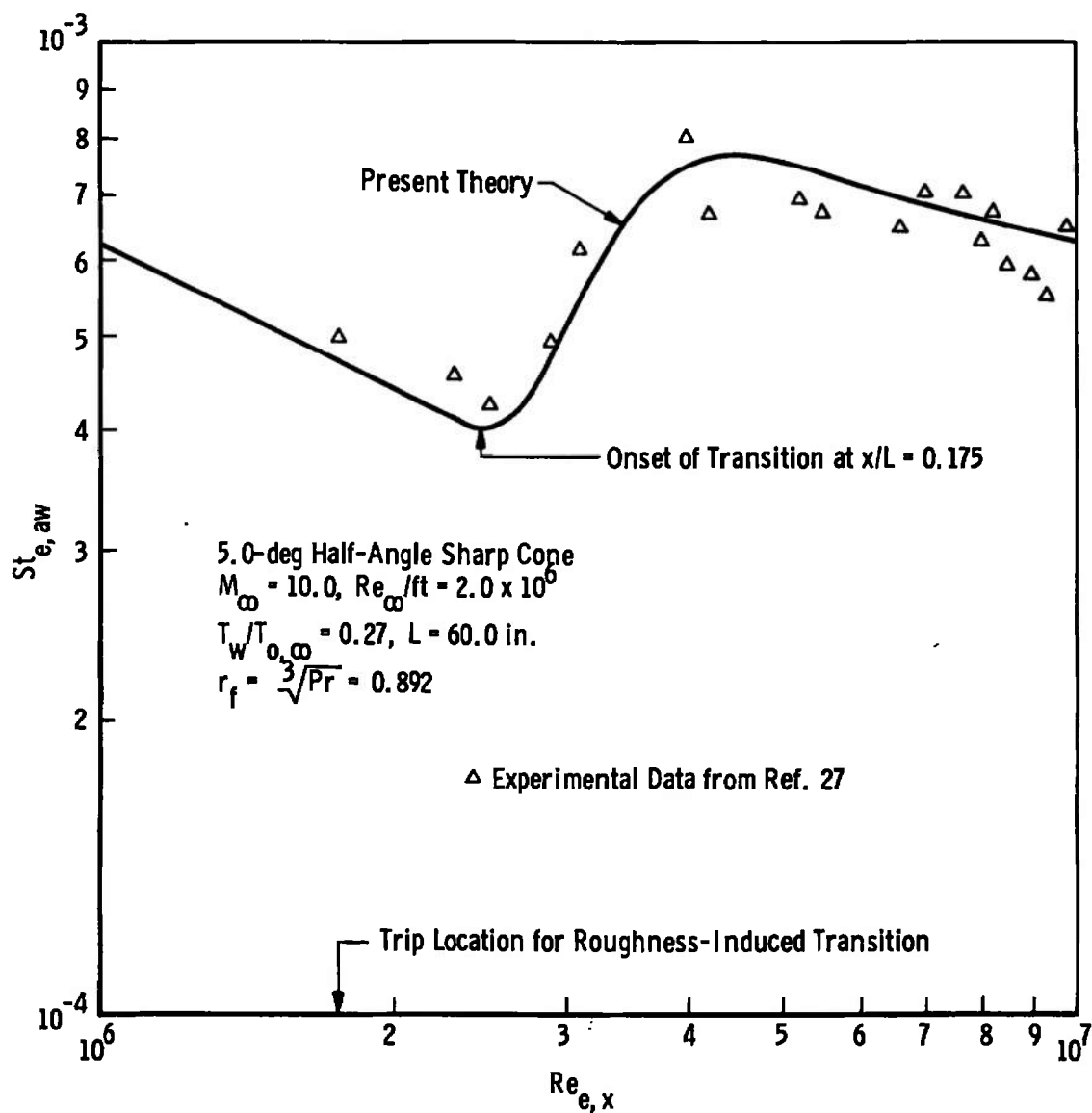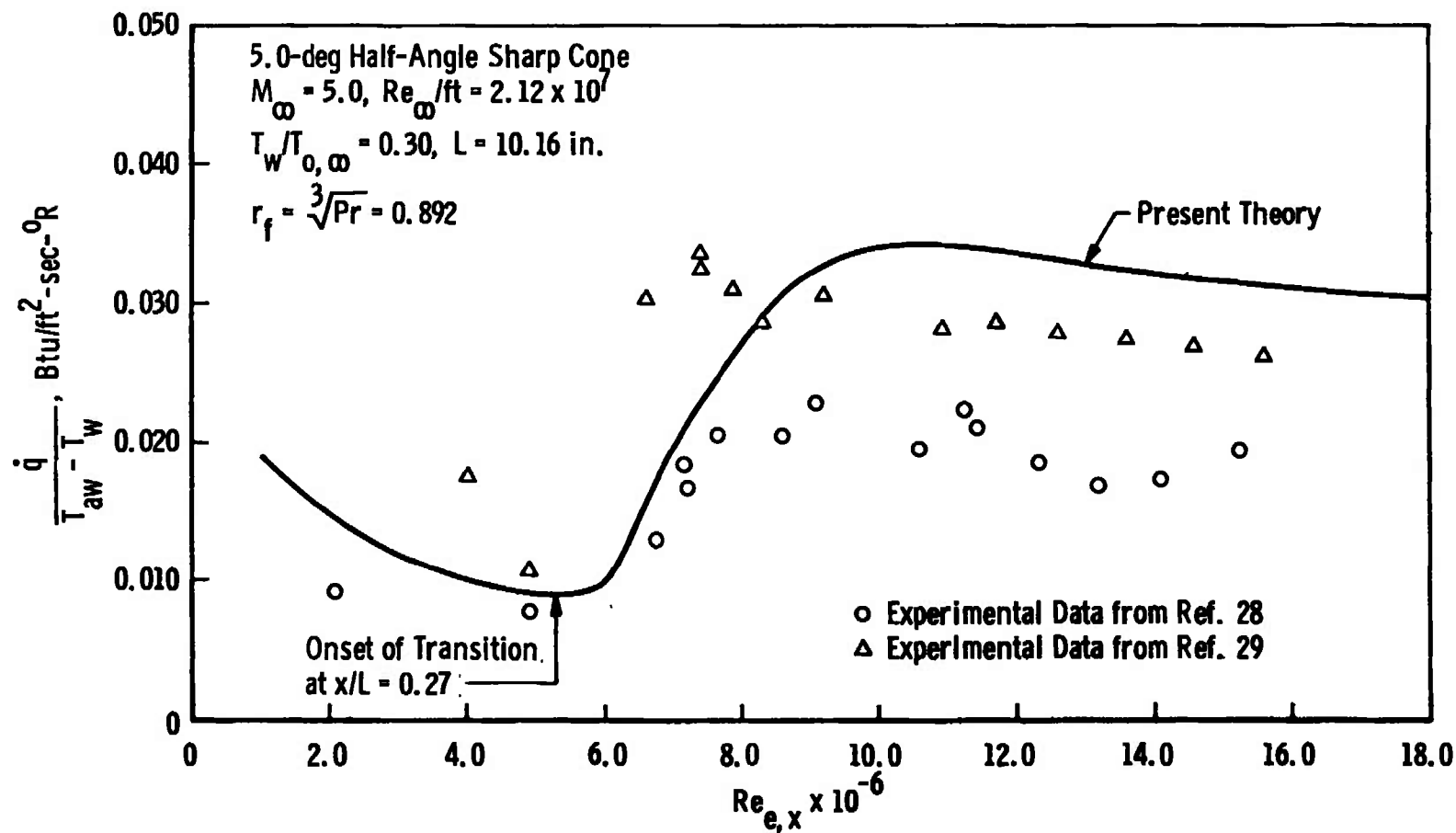| Ref.	δ_V, deg	M_∞	Re_∞/ft	$T_W/T_{0,\infty}$	$p_{0,\infty}$, psia	$T_{0,\infty}$, °R	L, in.
25	6.0	10.17	1.6×10^6	0.29	1310.0	1875.0	47.83
26	8.0	10.2	2.06×10^6	0.27	1710.0	1890.0	35.88
27	5.0	10.0	2.0×10^6	0.27	1666.0	2000.0	60.0
28	5.0	5.0	2.06×10^7	0.286	1176.0	1185.0	10.16
29	5.0	5.0	2.12×10^7	0.30	1176.0	1160.0	10.16
30	10.0	4.95	4.5×10^7	0.63	1545.0	860.0	5.76

TABLE II
SUMMARY OF INVISCID EDGE CONDITIONS USED IN COMPARISONS

Ref.	δ_V, deg	M_∞	p_e/p_∞	T_e/T_∞	M_e
25	6.0	10.17	2.87	1.38	8.58
26	8.0	10.2	4.19	1.60	7.94
27	5.0	10.0	2.31	1.28	8.77
28	5.0	5.0	1.40	1.10	4.71
29	5.0	5.0	1.40	1.10	4.71
30	10.0	4.95	2.03	1.15	4.55

APPENDIX III
IMPLICIT FINITE-DIFFERENCE SOLUTION OF GOVERNING BOUNDARY-LAYER EQUATIONS

For the special case of a sharp cone in a hypersonic flow, the inviscid flow field is conical in character so that all the inviscid flow parameters (p, T_e, ρ_e, U_e) remain constant along rays from the apex of the cone. Under this restriction the governing equations (43) and (44) in the transformed plane reduce to the following simpler set

MOMENTUM

$$\ell^* \; f''' \; + \left[\frac{\partial \ell^*}{\partial \eta} + f\right] f'' \; = 2\xi \left[f' \; \frac{\partial f'}{\partial \xi} - f'' \; \frac{\partial f}{\partial \xi}\right] \qquad \text{(III-1)}$$

ENERGY

$$\left(\frac{\ell^{**}}{Pr}\right)\theta'' + \left[\frac{\partial}{\partial \eta}\left(\frac{\ell^{**}}{Pr}\right) + f\right]\theta' \; + (\gamma-1)M_e^2 \; \ell^* \; (f'')^2$$

$$= 2\xi \left[f' \; \frac{\partial \theta}{\partial \xi} - \frac{\partial f}{\partial \xi} \; \theta' \right] \qquad \text{(III-2)}$$

which apply to any boundary-layer flow having constant inviscid flow parameters. The boundary conditions remain unchanged from Eqs. (52) through (56) which are repeated below for completeness.

MOMENTUM

$$f(\xi, \; \eta = 0) = 0 \qquad \text{(III-3)}$$

$$f'(\xi, \; \eta = 0) = 0 \qquad \text{(III-4)}$$

$$\lim_{\eta \to \infty} f'(\xi, \eta) = 1 \qquad \text{(III-5)}$$

ENERGY

$$\theta(\xi, \eta = 0) = \theta_W(\xi) \qquad \text{(III-6)}$$

$$\lim_{\eta \to \infty} \theta(\xi, \eta) = 1 \qquad \text{(III-7)}$$

Following the approach by Davis (Ref. 43) and Blottner (Ref. 44) the momentum and energy equations (Eqs. (III-1) and (III-2)) are rewritten in "standard" form for a parabolic partial differential equation as

$$\frac{\partial^2 W}{\partial \eta^2} + \alpha_1 \frac{\partial W}{\partial \eta} + \alpha_2 W + \alpha_3 + \alpha_4 \frac{\partial W}{\partial \xi} = 0 \qquad \text{(III-8)}$$

where $W = f'$ for the momentum equation and $W = \theta$ for the energy equation. Using Eqs. (III-1) and (III-2), the coefficients α_1 through α_4 are found to be, in linearized form:

MOMENTUM

$$\alpha_1 = \frac{\frac{\partial \ell^*}{\partial \eta} + f + 2\xi \frac{\partial f}{\partial \xi}}{\ell^*} \qquad \text{(III-9)}$$

$$\alpha_2 = 0 \qquad \text{(III-10)}$$

$$\alpha_3 = 0 \qquad \text{(III-11)}$$

$$\alpha_4 = \frac{-2\xi \, f'}{\ell^*} \qquad \text{(III-12)}$$

ENERGY

$$\alpha_1 = \frac{\frac{\partial}{\partial \eta}\left(\frac{\ell^{**}}{Pr}\right) + f + 2\xi \frac{\partial f}{\partial \xi}}{\left(\frac{\ell^{**}}{Pr}\right)} \qquad \text{(III-13)}$$

$$\alpha_2 = 0 \qquad \text{(III-14)}$$

$$\alpha_3 = \frac{(\gamma-1)M_e^2 \, \ell^* \, (f'')^2}{\left(\frac{\ell^{**}}{Pr}\right)} \qquad \text{(III-15)}$$

$$\alpha_4 = \frac{-2\xi \, f'}{\left(\frac{\ell^{**}}{Pr}\right)} \qquad \text{(III-16)}$$

The η derivatives in Eq. (III-8) are replaced with finite-difference quotients which allow variable grid spacing in the η direction so as to concentrate grid points in the region near the body surface where the dependent variables change most rapidly. The derivative in the ξ direction in Eq. (III-8) is handled in the usual manner as a two-point backward difference between points (m+1, n) and (m, n) while all η derivatives are evaluated at point (m+1, n) according to the grid mesh shown below.
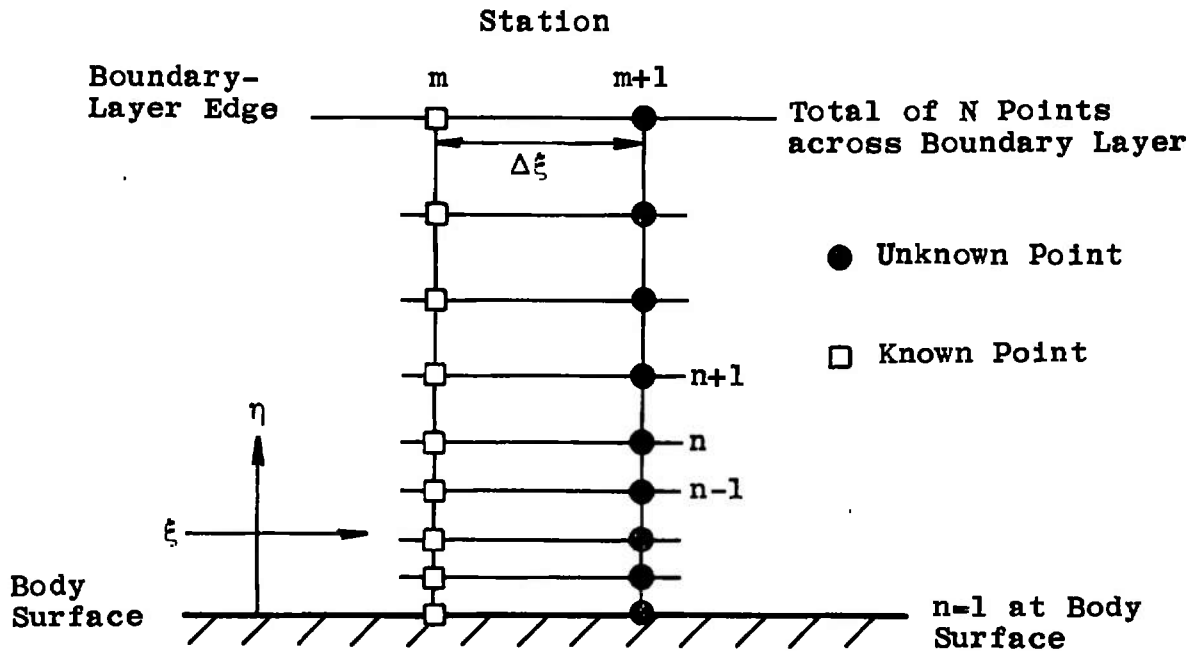
The solution is assumed to be known at point (m, n) and unknown at point (m+1, n) so that the finite-difference scheme to be constructed will be implicit in nature. The finite-difference replacements for the derivatives are as follows:

$$\frac{\partial^2 W}{\partial \eta^2}\bigg]_{m+1,n} = \frac{2[W_{n+1} + KW_{n-1} - (1+K)W_n]_{m+1}}{D_2} \qquad \text{(III-17)}$$

61

$$\frac{\partial W}{\partial \eta}\Bigg]_{m+1,n} = \frac{[W_{n+1} - K^2 W_{n-1} - (1-K^2)W_n]_{m+1}}{D_1} \qquad \text{(III-18)}$$

$$\frac{\partial W}{\partial \xi}\Bigg]_{m+1,n} = \frac{W_{m+1,n} - W_{m,n}}{\Delta \xi} \qquad \text{(III-19)}$$

where

$$D_1 = (\eta_{n+1} - \eta_n) + K^2(\eta_n - \eta_{n-1}) \qquad \text{(III-20)}$$

$$D_2 = (\eta_{n+1} - \eta_n)^2 + K(\eta_n - \eta_{n-1})^2 \qquad \text{(III-21)}$$

$$K = \frac{\eta_{n+1} - \eta_n}{\eta_n - \eta_{n-1}} \quad \text{(constant)} \qquad \text{(III-22)}$$

$$\Omega = \eta_2 - \eta_1 \quad \text{(constant)} \qquad \text{(III-23)}$$

The finite-difference form of Eq. (III-8) becomes, upon substitution of Eqs. (III-17), (III-18), and (III-19),

$$A_n \, W_{m+1,n+1} + B_n \, W_{m+1,n} + C_n \, W_{m+1,n-1} = R_n \qquad \text{(III-24)}$$

where

$$A_n = \frac{2}{D_2} + \frac{\alpha_1}{D_1} \qquad \text{(III-25)}$$

$$B_n = \frac{-2(1+K)}{D_2} - \frac{\alpha_1(1-K^2)}{D_1} + \alpha_2 + \frac{\alpha_4}{\Delta \xi} \qquad \text{(III-26)}$$

$$C_n = \frac{2K}{D_2} - \frac{K^2 \alpha_1}{D_1} \qquad \text{(III-27)}$$

$$R_n = -\alpha_3 + \frac{\alpha_4 \, W_{m,n}}{\Delta \xi} \qquad \text{(III-28)}$$

In order for Eq. (III-24) to be linear, the coefficients A_n, B_n, C_n, and R_n must be treated as known quantities at point n; more will follow

on this subject later. The important point is that Eq. (III-24) represents a set of simultaneous linear algebraic equations under this restriction.

Since the simultaneous linear algebraic equations resulting from Eq. (III-24) are of a special form (tridiagonal), an efficient method of solution on a digital computer is available from Richtmyer and Morton (Ref. 45, pp. 198 to 201 and 274 to 282). For this procedure the boundary conditions at the wall (n = 1) and the outer edge (n = N) must have specified values $W_{m+1, 1}$ and $W_{m+1, N}$. Because of the special form of Eq. (III-24), the relation

$$W_{m+1,n} = E_n W_{m+1,n+1} + e_n, \quad 2 \leqq n \leqq N-1 \qquad \text{(III-29)}$$

exists where

$$E_2 = \frac{-A_2}{B_2} \qquad \text{(III-30)}$$

$$e_2 = \frac{R_2 - C_2 W_{m+1,1}}{B_2} \qquad \text{(III-31)}$$

$$\left. \begin{aligned} E_n &= \frac{-A_n}{B_n + C_n E_{n-1}} \qquad \text{(III-32)} \\[2em] e_n &= \frac{R_n - C_n e_{n-1}}{B_n + C_n E_{n-1}} \qquad \text{(III-33)} \end{aligned} \right\} \quad 3 \leqq n \leqq N-1$$

The quantities E_n and e_n are computed from Eqs. (III-30) through (III-33) starting with n = 2 and progressing to n = N-1. The solution $W_{m+1, n}$ is then obtained by evaluating Eq. (III-29) from n = N - 1 to n = 2. Knowing the distribution of f' and θ across the boundary layer from the above procedure, the transformed stream function f is evaluated from

$$f(\xi,\eta) = \int_0^\eta f'(\xi,\eta)d\eta \qquad \text{(III-34)}$$

where the integral is numerically integrated using the well-known trapezoidal rule, viz

$$f(\xi, n = n_n) = \sum_{i=2}^{n} \left[f'(\xi, n = n_i) + f'(\xi, n = n_{i-1}) \right] D_i \quad \text{(III-35)}$$

with

$$D_i = \frac{n_i - n_{i-1}}{2} \quad \text{(III-36)}$$

In a similar manner, the inversion from the transformed (ξ, η) plane to the physical (x, y) plane is, from Eq. (37),

$$y = \frac{\sqrt{2\xi}}{\rho_e U_e r_b^j} \int_0^n \frac{\rho_e}{\rho} \, dn \quad \text{(III-37)}$$

where

$$\frac{\rho_e}{\rho} = \frac{T}{T_e} = \theta \quad \text{(III-38)}$$

because of the constancy of static pressure across the boundary layer. Again, using the trapezoidal rule method of numerical integration yields

$$y_n = \frac{\sqrt{2\xi}}{\rho_e U_e r_b^j} \sum_{i=2}^{n} \left[\theta(\xi, n = n_i) + \theta(\xi, n = n_{i-1}) \right] D_i \quad \text{(III-39)}$$

with D_i given by Eq. (III-36). The relationship between ξ and x for sharp cone flows is found by integration of Eq. (36) with $r_b^j = x \sin \delta_v$ from geometry which results in

$$\xi = \frac{1}{3} \rho_e \mu_e U_e \sin^2 \delta_v x^3 \quad \text{(III-40)}$$

For the present work the $\Delta\xi$ increment of integration is chosen based on the division $\Delta x = 0.01 L$, i.e., 100 stations spaced equally along the physical body.

The mathematical basis of the above tridiagonal matrix procedure applied to the solution of boundary-layer problems is attributable to Flügge-Lotz and Blottner (Ref. 46). The present application differs from their original work in one important aspect: the linearized difference equations herein are uncoupled and solved separately. In

64

Flügge-Lotz and Blottner's approach, the difference equations remain coupled and require additional machine storage and manipulations for solution. With the present uncoupled approach, the difference equations are iterated to convergence at each station along the body so that one must pay the price of iteration; this procedure is how the linearizing coefficients α_1 through α_4 are evaluated at each station using the results of the previous iteration. Hence the final solution obtained at each station is exact in the sense that it represents a converged iterated solution to the governing nonlinear partial differential equations written in finite-difference form. Typically about three iterations per station are required for fully turbulent flow; only one to two iterations per station are necessary for laminar flow.

The variable grid mesh used in the present work is taken from Smith and Cebeci (Ref. 2). The various constants used herein are as follows:

$$N = 85$$

$$K = 1.063$$

$$\Omega = 0.010$$

Experience with varying these constants and observing their influence on the resultant numerical solution has indicated that the above choices are adequate under the present flow conditions. These values may not be satisfactory, however, for other body geometries and flow conditions so that the influence of the variable grid mesh constants should be ascertained for each new investigation. Provisions are included in the present program for addition of points (if necessary) to the solution as the body is traversed. This may be required in order to prevent numerical suppression of boundary-layer growth.

At the apex of a sharp cone where $\xi = 0$, the governing boundary-layer equations (Eqs. (III-1) and (III-2)) reduce to the following ordinary, nonlinear, differential equations

MOMENTUM

$$\ell^* \, f''' + \left[\frac{\partial \ell^*}{\partial \eta} + f \right] f'' = 0 \tag{III-41}$$

ENERGY

$$\left(\frac{\ell^{**}}{Pr}\right)\theta'' + \left[\frac{\partial}{\partial\eta}\left(\frac{\ell^{**}}{Pr}\right) + f\right]\theta' \tag{III-42}$$

$$+ (\gamma-1)M_e^2 \ell^* (f'')^2 = 0$$

with the boundary conditions of Eqs. (III-3) through (III-7). In order to obtain starting profiles for the finite-difference scheme to march downstream, Eqs. (III-41) and (III-42) are solved by using the tridiagonal matrix procedure described previously in the following manner. At the apex of the cone $\xi = 0$ so that $\alpha_4 = 0$ in both the momentum and energy equations; in addition, the term containing ξ in α_1 of both the momentum and energy equation vanishes. Initial guesses for f' and θ are input to the program as

$$f'_I = 1 - \exp(-\eta) \tag{III-43}$$

$$\theta_I = \theta_w + (1 - \theta_w)f'_I \tag{III-44}$$

where the subscript I denotes the initial approximation. The equations are then iterated to convergence in the same manner described previously; an averaging scheme is used to speed convergence. Typically, about 20 to 25 iterations are required to generate a converged initial solution.

By use of the above procedures, the numerical solution of any two-point boundary-value problem governed by either linear or nonlinear ordinary differential equations as well as sets of coupled parabolic partial differential equations, either linear or nonlinear, is reduced to subroutine status on a digital computer in that only the coefficients α_1 through α_4 must be defined in conjunction with the required boundary conditions for each new problem. Much application of these procedures has been found in the von Kármán Gas Dynamics Facility of the Arnold Engineering Development Center on many different problems involving both nonlinear, ordinary, differential equations as well as parabolic, partial, differential equations. The thin viscous shock layer analysis by Adams (Ref. 47) is a good example. In this work eight simultaneous, nonlinear, ordinary, differential equations governing momentum, energy, and species conservation were solved using the iterative tridiagonal matrix method presented above. The problem was made even more difficult in that chemical nonequilibrium effects were included in the analysis. Based on experience with analyses of this type, the author highly recommends use of the iterative tridiagonal matrix approach where applicable.

DOCUMENT CONTROL DATA - R & D

(Security classification of title, body of abstract and indexing annotation must be entered when the overall report is classified)

1. ORIGINATING ACTIVITY (Corporate author)	2a. REPORT SECURITY CLASSIFICATION
Arnold Engineering Development Center ARO, Inc., Operating Contractor Arnold Air Force Station, Tennessee 37389	UNCLASSIFIED
	2b. GROUP N/A

3 REPORT TITLE

EDDY VISCOSITY-INTERMITTENCY FACTOR APPROACH TO NUMERICAL CALCULATION OF TRANSITIONAL HEATING ON SHARP CONES IN HYPERSONIC FLOW

4 DESCRIPTIVE NOTES *(Type of report and inclusive dates)*

Final Report   July 1969 to March 1970

5. AUTHOR(S) *(First name, middle initial, last name)*

John C. Adams, Jr., ARO, Inc.

6. REPORT DATE	7a. TOTAL NO. OF PAGES	7b. NO. OF REFS
November 1970	76	47

8a. CONTRACT OR GRANT NO. F40600-71-C-0002	9a. ORIGINATOR'S REPORT NUMBER(S)
b. PROJECT NO. 8953	AEDC-TR-70-210
c. Program Element 62201F	9b. OTHER REPORT NO(S) (Any other numbers that may be assigned this report)
d. Task 03	ARO-VKF-TR-70-198

10. DISTRIBUTION STATEMENT

This document has been approved for public release and sale; its distribution is unlimited.

11 SUPPLEMENTARY NOTES	12. SPONSORING MILITARY ACTIVITY
Available in DDC	Arnold Engineering Development Center, AFSC, Arnold Air Force Station, Tennessee 37389

13 ABSTRACT

Analysis of laminar, transitional, and turbulent boundary layers on a sharp cone at zero angle of attack under hypersonic perfect gas conditions is presented. The governing boundary-layer equations were numerically integrated on a digital computer using a marching, iterative, implicit, finite-difference method. The turbulent boundary layer is analyzed using a two-layer eddy viscosity model with a constant turbulent Prandtl number, and the transition region is treated through an eddy viscosity-intermittency factor approach. Comparison with experimental data reveals that the present approach yields an accurate description of laminar, transitional, and fully turbulent heat transfer on sharp cones in the Mach number range from 5 to 10 under cold wall conditions. Verification of the detailed calculation of transitional and turbulent boundary-layer structure under hypersonic conditions must await further experimental investigations. It appears at the present time that the eddy viscosity approach to calculation of transitional and turbulent boundary layers may indeed be applicable and accurate under hypersonic conditions.

DD FORM 1473 1 NOV 65

14. KEY WORDS	LINK A		LINK B		LINK C	
	ROLE	WT	ROLE	WT	ROLE	WT
conical bodies						
hypersonic flow						
transition flow						
heat transfer						
laminar flow						
turbulent flow						
boundary layer transition						
viscosity						
computation						

1. Cones -- Turbulent boundary layer
    -- Boundary layer transition

2. "
    -- Heat Transfer

3. "

AFSC
Arnold AFS Tenn